



 Cite this: *RSC Adv.*, 2026, 16, 8466

Design, synthesis, structural characterization, anticancer evaluation, and computational studies of novel quinoline-1,2,3-triazole glycohybrids

 Ravendra Kumar,^a Deepanshi Chauhan,^a Rakesh Kumar Gupta,^b Pawan K. Dubey^b and Divya Kushwaha *^a

A novel series of eleven phenyl-substituted quinoline 1,2,3-triazole glycoconjugates **6(a–k)** was synthesized via the copper(I)-catalyzed azide-alkyne cycloaddition (CuAAC) reaction between 2-phenyl-substituted quinoline-4-carboxylic acid propargyl ester (**4a–4e**) and various sugar azides (**5a**, **5b**, and **5c**). The obtained compounds were comprehensively characterized by FT-IR, ¹H NMR, ¹³C NMR, and mass spectrometry. The chemical structures of compounds **6a**, **6b**, and **6e** were further established by single-crystal X-ray diffraction analysis. Their crystal packing was stabilized through a network of intermolecular hydrogen bonds involving C–H⋯N, N–H⋯N, and C–H⋯O (sp², sp³) interactions, which were qualitatively analyzed using Hirshfeld surface analysis. *In vitro* anticancer evaluation against the MCF-7 breast cancer cell line revealed that most of the compounds of the series were inactive, while compounds **6c**, **6d**, and **6f** exhibited only weakly cytotoxic activity (IC₅₀ values of 108.59–135.95 μM). Molecular docking with estrogen receptor alpha (ERα, PDB ID: 3ERT) revealed good binding affinities (up to –9.1 kcal mol^{–1}), comparable to the reference ligand (–9.7 kcal mol^{–1}). Furthermore, DFT calculations were performed to evaluate key electronic parameters (HOMO–LUMO energies, reactivity, stability, and charge distribution), offering insight into the compounds' chemical behaviour and electronic properties.

 Received 15th December 2025
 Accepted 27th January 2026

DOI: 10.1039/d5ra09700b

rsc.li/rsc-advances

1. Introduction

Quinoline derivatives constitute an important class of heterocyclic compounds that have attracted considerable attention due to their broad spectrum of pharmacological activities, including anticancer, antimicrobial, antioxidant, antitubercular, antidiabetic, antimycobacterial, anticonvulsant, anti-Alzheimer, anti-inflammatory, and cardiovascular properties.¹ Classical synthetic strategies such as the Pfitzinger and Friedländer reactions have long served as fundamental approaches for constructing quinoline frameworks with structural diversity. Owing to the remarkable structural versatility and diverse biological relevance, quinoline-based scaffolds have been extensively investigated in medicinal chemistry for the development of novel therapeutic agents, particularly anticancer drugs.² Quinoline-based compounds are known to exert anticancer activity through multiple mechanisms, including inhibition of tyrosine kinases, cell cycle arrest, suppression of angiogenesis, induction of apoptosis, inhibition of tubulin polymerization, and disruption of cell migration *etc.*³ Furthermore, structural modification of the quinoline nucleus has

yielded numerous derivatives with enhanced potency, particularly through DNA intercalation and interference with replication processes, emphasizing the significance of quinoline scaffold as versatile pharmacophore for anticancer drug design.^{2,3}

To enhance the therapeutic potential of a bioactive heterocycle, molecular hybridization strategies have gained increasing attention, notably through the copper(I)-catalyzed azide-alkyne cycloaddition (CuAAC). This highly efficient and regioselective click reaction enables the reliable conjugation of two structurally and functionally distinct pharmacophoric moieties.^{4,5} The resulting 1,2,3-triazole linker exhibits remarkable chemical stability and acts as a bioisostere for amide and ester linkages, improving molecular polarity, hydrogen-bonding ability, and pharmacokinetic behaviour.^{6–8} Additionally, the conjugation of heterocyclic frameworks with carbohydrates has emerged as an effective approach in modern drug design due to their inherent chirality, hydrophilicity, target selectivity, and critical roles in molecular recognition and cellular processes.^{9,10} Such glycohybrid systems exploit the elevated glucose uptake rate of cancer cells, facilitating selective accumulation within tumour tissues and thereby improving therapeutic efficacy.

Breast cancer remains one of the most prevalent malignancies worldwide and represents the second leading cause of cancer-related mortality, accounting for approximately 24% of all diagnosed cancer cases and 15% of associated deaths.¹¹ It is

^aDepartment of Chemistry, MMV, Banaras Hindu University, Varanasi-221005, India. E-mail: divyakush.mmvbhu@ac.in

^bCentre for Genetic Disorder, Institute of Science, Banaras Hindu University, Varanasi-221005, India



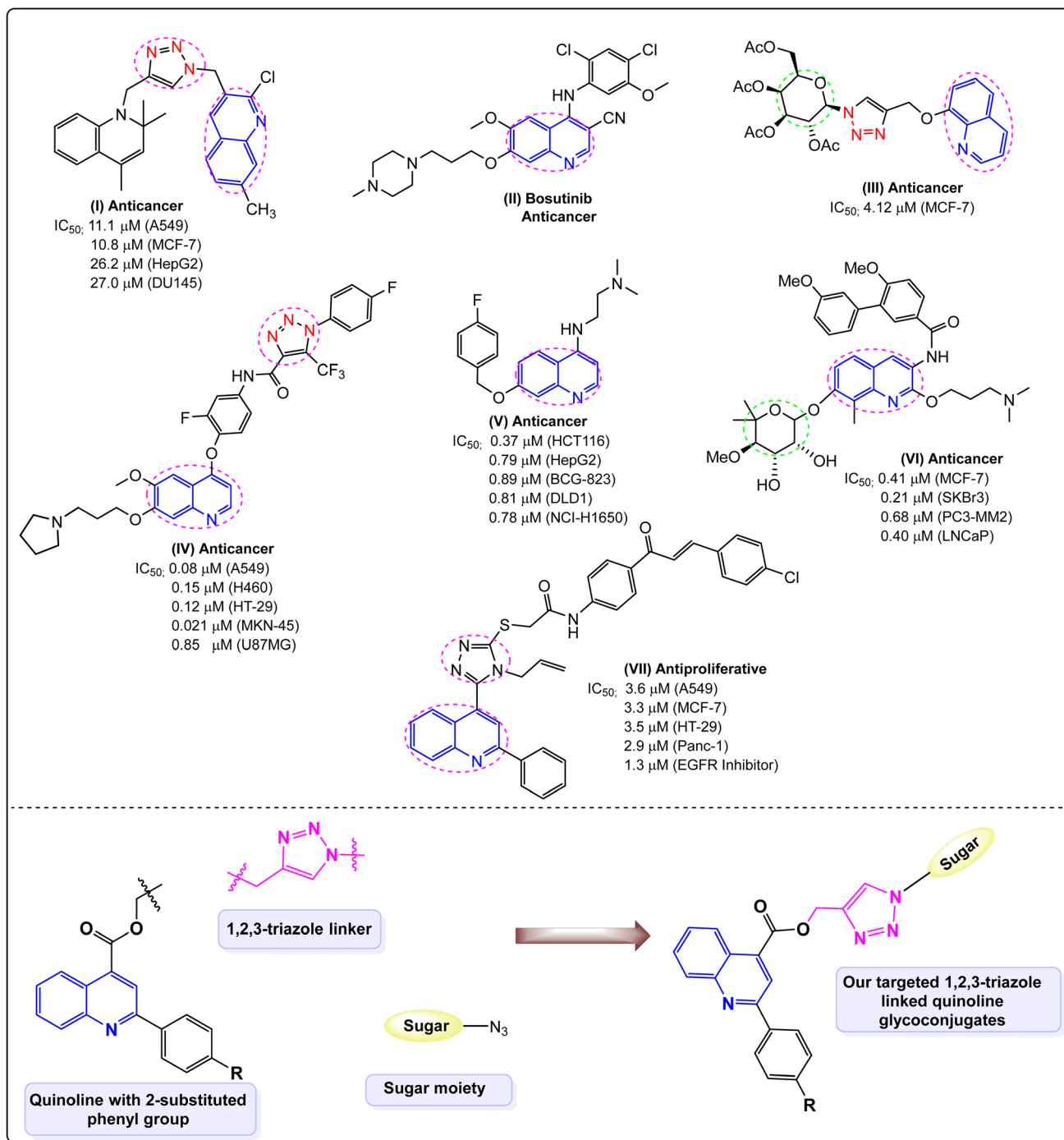


Fig. 1 Previously reported quinoline triazole derivatives with potent anticancer activity I–VII and our synthesized 2-phenylquinoline glycoconjugates.

recognized as a heterogeneous disease comprising multiple molecular subtypes including, luminal A, luminal B, human epidermal growth factor (HER2)-positive, and triple-negative.¹² The MCF-7 cell line, established in 1973, serves as a representative model of luminal A-type breast cancer characterized by estrogen receptor (ER α)- and progesterone receptor (PR)-positive, low invasiveness and limited metastatic potential.¹³

Numerous quinoline- and 1,2,3-triazole-based compounds (I–VII) reported in the literature have exhibited notable

anticancer activity, highlighting these motifs as privileged scaffolds in anticancer drug design (Fig. 1). Compound I, a 1,4-disubstituted 1,2,3-triazole derivative featuring a quinolinylmethylene group at the N-1 position and a 1,2-dihydroquinolinylmethylene group at the C-4 position, demonstrated significant cytotoxic activity against lung cancer cells. Additionally, its ability to inhibit phosphodiesterase 4 (PDE4) highlights its potential as a promising anticancer candidate.¹⁴ The compound II, known as SKI-606 (bosutinib), is a quinoline-

based anticancer agent that effectively inhibits Src-mediated signalling pathways, thereby suppressing the migration and invasion of breast cancer cells.¹⁵ The compound **III**, a 1,2,3-triazole-linked quinoline glycoconjugate, showed potent anticancer activity against MCF-7 cells. The 1,2,3-triazole moiety enhanced cytotoxicity, and the combination of the 8-hydroxyquinoline core, acetyl-protected sugar, and triazole linker was key to its activity.¹⁶ The compound **IV**, a quinoline-based 1,2,3-triazole-4-carboxamide, showed potent antitumor activity, with a 4-fluoro substituent on the phenyl ring and a trifluoromethyl group at C-5 of triazole enhanced c-Met inhibition and cytotoxicity.¹⁷ In 2018, Li *et al.* reported that compound **V**, featuring a bulky alkoxy group at the 7-position and amino side chains at the 4-position with an optimal two-CH₂ unit length, demonstrated strong anticancer activity against colorectal cancer cells by triggering p53/Bax-mediated apoptosis through the activation of p53 transcriptional signaling.¹⁸ Kusuma *et al.* developed novobiocin analogues by replacing the coumarin framework with a quinoline scaffold to assess their anticancer potential through Hsp90 inhibition. Among these, compound **VI** displayed notable antiproliferative effects across various cancer cell lines, identifying 2-alkoxyquinoline derivatives as key active structures.¹⁹ Compound **VII**, a quinoline-chalcone-triazole hybrid, showed the most potent antiproliferative activity against multiple cancer cell lines, in which the presence of the allyl and triazole moieties played a crucial role in enhancing the biological activity. It also inhibited EGFR and BRAF kinases and induced apoptosis with G2/M phase arrest in Panc-1 cells, confirming its strong anticancer potential.²⁰

In light of these reported studies, the present work describes the synthesis and characterization of a series of 2-phenyl derivatives of quinoline-4-carboxy 1,2,3-triazole glycoconjugates **6(a-k)**. Single-crystal X-ray diffraction analysis was carried out to elucidate the solid-state structures of compounds **6a**, **6b**, and **6e**. The anticancer potential of the compounds was subsequently evaluated *in vitro* against the MCF-7 human breast cancer cell line. Furthermore, comprehensive computational studies were carried out to assess the chemical stability, electronic properties, and binding interactions of the synthesized derivatives with the estrogen receptor alpha (ER α ; PDB ID: 3ERT).

2. Experimental section

2.1. General experimental methods

All experiments were performed using analytical grade reagents and solvents without further purification. Thin-layer chromatography (TLC) was conducted on silica gel 60-F₂₅₄ pre-coated aluminium plates (0.25 mm), and spots were visualized under UV light, by exposure to iodine vapours, or by charring after spraying with 5% H₂SO₄ in methanol. Column chromatography was carried out on silica gel (230–400 mesh) using suitable solvent systems. Melting points were determined in open capillaries using a digital melting point apparatus. IR spectra were recorded on a Bruker FTIR 5300 spectrophotometer using KBr pellets (4000–400 cm⁻¹). ¹H and ¹³C NMR spectra were obtained on JEOL (500/125 MHz) and Bruker (600/150 MHz)

spectrometers. Chemical shifts (δ) are given in ppm relative to TMS, and coupling constants (J) in Hz. The following abbreviations are used: s = singlet, d = doublet, t = triplet, dd = double doublet, m = multiplet, br s = broad singlet. HRMS data were recorded on an X500-QTOF mass spectrometer with an electrospray ionization (ESI) source.

2.2. General experimental procedure for the synthesis of 3(a–e)

Isatin (**1**, 10 mmol) was dissolved in a stirred mixture of 33% aq. potassium hydroxide (10 mL) and ethanol (20 mL). To this solution, an appropriate acetophenone derivative (**2a–2e**, 10 mmol) was added, and the reaction mixture was refluxed for 18 h. The reaction mixture was cooled to room temperature and solvent was evaporated under reduced pressure. The aqueous layer was collected, cooled to 0 °C, and acidified dropwise with concentrated HCl until precipitation occurred (pH ~2). The resulting solid was filtered, washed with brine and then with cold ethanol, and dried. Recrystallization from ethanol afforded a light brown solid in good yield. Other derivatives (**3b–3e**) were synthesized using the same procedure, giving yields up to 88%.²¹

2.2.1. 2-Phenylquinoline-4-carboxylic acid (3a). Yield: 2.10 g (86%); m.p. 196–198 °C; R_f 0.30 (2 : 8, MeOH : CHCl₃, v/v); ¹H NMR (500 MHz, CDCl₃): δ_{ppm} = 8.76 (d, J = 8.9 Hz, 1H), 8.38 (s, 1H), 8.11 (d, J = 7.9 Hz, 3H), 7.66 (t, J = 7.9 Hz, 1H), 7.51 (t, J = 7.9 Hz, 1H), 7.44 (t, J = 7.4 Hz, 2H), 7.38 (t, J = 7.3 Hz, 1H); ¹³C NMR (150 MHz, CDCl₃): δ = 168.27, 156.47, 149.0, 138.66, 136.66, 129.91, 129.55, 129.47, 128.71, 127.32, 127.24, 125.64, 124.09, 120.21; HRMS (ESI): m/z calculated for C₁₆H₁₂NO₂, [M + H]⁺ 250.0790, found 250.0837, m/z calculated for C₁₆H₁₁NNaO₂, [M + Na]⁺ 272.0687, found 272.0683.

2.3. General experimental procedure for the synthesis of 4(a–e)

To a solution of 2-phenylquinoline-4-carboxylic acid **3a** (1.69 mmol, 1.0 equiv.) in dry dimethylformamide (DMF), and alcoholic sodium carbonate (Na₂CO₃, 2.03 mmol, 1.2 equiv.) was added as a base in a round-bottom flask. Subsequently, propargyl bromide (1.69 mmol, 1.0 equiv.) was added dropwise to the reaction mixture, which was then stirred at room temperature for 5 h. The progress of the reaction was monitored by thin-layer chromatography (TLC) using a 40% ethyl acetate and hexane solvent system. Upon completion, the reaction mixture was diluted with ethyl acetate, and the organic layer was sequentially washed with brine and dried over anhydrous sodium sulphate. The solvent was evaporated under reduced pressure to obtain the crude product, which was purified by column chromatography using 20% ethyl acetate in hexane as the eluent. All other derivatives were synthesized using the same standardized procedure, affording yields of up to 86%.

2.3.1. Prop-2-yn-1-yl 2-phenylquinoline-4-carboxylate (4a). A solution of 2-phenylquinoline-4-carboxylic acid **3a** (0.400 g, 1.695 mmol, 1.0 equiv.), propargyl bromide (0.128 mL, 2.03 mmol, 1.2 equiv.), 3 mL alcoholic Na₂CO₃ solution (0.234 g, 1.695 mmol, 1.0 equiv.) was prepared in 4 mL dry dimethyl



formamide and reacted as described above. After chromatographic purification **4a** was obtained. Light brown powder; yield 0.414 g (85%); m.p. 90–92 °C; R_f 0.30 (2 : 8, EtOAc/hexane v/v); ^1H NMR (600 MHz, CDCl_3): δ = 8.77 (d, J = 8.5 Hz, 1H), 8.44 (s, 1H), 8.25–8.21 (m, 3H), 7.78 (t, J = 7.7 Hz, 1H), 7.64 (t, J = 7.7 Hz, 1H), 7.55 (t, J = 7.6 Hz, 2H), 7.50 (t, J = 7.3 Hz, 1H), 5.08 (d, J = 2.5 Hz, 2H), 2.61 (t, J = 2.5 Hz, 1H); ^{13}C NMR (150 MHz, CDCl_3): δ = 165.63, 156.85, 149.40, 138.81, 134.83, 130.51, 130.15, 129.93, 129.09, 128.14, 127.62, 125.41, 124.03, 120.70, 77.32, 75.86, 53.25; HRMS (ESI): m/z calculated for $\text{C}_{19}\text{H}_{14}\text{NO}_2$, $[\text{M} + \text{H}]^+$ 288.0946, found 288.1012.

2.3.2. Prop-2-yn-1-yl 2-(4-chlorophenyl) quinoline-4-carboxylate (4b). A solution of 2-(4-chlorophenyl) quinoline-4-carboxylic acid **3b** (0.350 g, 1.233 mmol, 1.0 equiv.), propargyl bromide (0.093 mL, 1.233 mmol, 1.0 equiv.), 2 mL alcoholic Na_2CO_3 solution (0.170 g, 1.233 mmol, 1.0 equiv.), was prepared in 4 mL dry dimethyl formamide and reacted as described above. After chromatographic purification **4b** was obtained. Yellowish crystalline powder; yield 0.341 g (86%); m.p. 103–105 °C; R_f 0.35 (2 : 8, EtOAc/hexane v/v); ^1H NMR (500 MHz, CDCl_3): δ = 8.77 (d, J = 9.3 Hz, 1H), 8.40 (s, 1H), 8.21 (d, J = 8.0 Hz, 1H), 8.17 (d, J = 9.3 Hz, 2H), 7.79 (t, J = 7.3 Hz, 1H), 7.66 (t, J = 7.3 Hz, 1H), 7.52 (d, J = 8.0 Hz, 2H), 5.08 (s, 2H), 2.61 (s, 1H); ^{13}C NMR (125 MHz, CDCl_3): δ = 165.54, 155.55, 149.42, 137.24, 136.26, 135.10, 130.52, 130.35, 129.31, 128.90, 128.37, 125.48, 124.12, 120.23, 77.28, 75.92, 53.32; HRMS (ESI): m/z calculated for $\text{C}_{19}\text{H}_{13}\text{ClNO}_2$, $[\text{M} + \text{H}]^+$ 322.0557, found 322.0606.

2.3.3. Prop-2-yn-1-yl 2-(4-methoxyphenyl) quinoline-4-carboxylate (4c). A solution of 2-(4-methoxyphenyl) quinoline-4-carboxylic acid **3c** (0.300 g, 1.074 mmol, 1.0 equiv.), propargyl bromide (0.081 mL, 1.047 mmol, 1.0 equiv.), 1.5 mL alcoholic Na_2CO_3 solution (0.148 g, 1.047 mmol, 1.0 equiv.), was prepared in 4 mL dry dimethyl formamide and reacted as described above. After chromatographic purification **4c** was obtained. Reddish brown powder; yield 0.286 g (84%); m.p. 100–102 °C; R_f 0.40 (2 : 8, EtOAc/hexane v/v); ^1H NMR (600 MHz, CDCl_3): δ = 8.73 (d, J = 7.0 Hz, 1H), 8.39 (s, 1H), 8.20–8.18 (m, 3H), 7.75 (t, J = 6.9 Hz, 1H), 7.60 (t, J = 7.0 Hz, 1H), 7.07–7.05 (m, 2H), 5.07 (d, J = 2.5 Hz, 2H), 3.89 (s, 3H), 2.60 (t, J = 2.5 Hz, 1H); ^{13}C NMR (150 MHz, CDCl_3): δ = 165.72, 161.32, 156.38, 149.39, 134.69, 131.37, 130.28, 130.06, 129.00, 127.70, 125.38, 123.69, 120.28, 114.47, 75.82, 55.55, 53.20; HRMS (ESI): m/z calculated for $\text{C}_{20}\text{H}_{16}\text{NO}_3$, $[\text{M} + \text{H}]^+$ 318.1052, found 318.1108.

2.3.4. Prop-2-yn-1-yl 2-(4-fluorophenyl) quinoline-4-carboxylate (4d). A solution of 2-(4-fluorophenyl) quinoline-4-carboxylic acid **3d** (0.400 g, 1.491 mmol, 1.0 equiv.), propargyl bromide (0.113 mL, 1.491 mmol, 1.0 equiv.), 2 mL alcoholic Na_2CO_3 solution (0.206 g, 1.491 mmol, 1.0 equiv.), was prepared in 5 mL dry dimethyl formamide and reacted as described above. After chromatographic purification **4d** was obtained. Brownish powder; yield 0.388 g (85%); m.p. 95–97 °C; R_f 0.35 (2 : 8, EtOAc/hexane v/v); ^1H NMR (600 MHz, CDCl_3): δ = 8.75 (d, J = 7.2 Hz, 1H), 8.38 (d, J = 2.6 Hz, 1H), 8.21–8.19 (m, 2H), 7.77 (t, J = 6.9 Hz, 1H), 7.63 (t, J = 7.0 Hz, 1H), 7.22 (t, J = 8.6 Hz, 2H), 7.04 (d, J = 8.8 Hz, 1H), 5.07 (d, J = 2.6 Hz, 2H), 2.61 (t, J = 2.5 Hz, 1H); ^{13}C NMR (150 MHz, CDCl_3): δ = 165.52, 155.66, 149.38, 134.94, 130.39, 130.25, 129.54, 129.49, 128.96, 128.17,

125.42, 123.91, 120.26, 116.11, 115.97, 114.97, 77.26, 75.90, 53.18; HRMS (ESI): m/z calculated for $\text{C}_{19}\text{H}_{13}\text{FNO}_2$, $[\text{M} + \text{H}]^+$ 306.0852, found 306.0921.

2.3.5. Prop-2-yn-1-yl 2-(4-methylphenyl) quinoline-4-carboxylate (4e). A solution of 2-(4-methylphenyl) quinoline-4-carboxylic acid **3e** (0.450 g, 1.709 mmol, 1.0 equiv.), propargyl bromide (0.129 mL, 1.709 mmol, 1.0 equiv.), 2 mL alcoholic Na_2CO_3 solution (0.236 g, 1.709 mmol, 1.0 equiv.), was prepared in 5 mL dry dimethyl formamide and reacted as described above. After chromatographic purification **4e** was obtained. Brownish powder; yield 0.433 g (86%); m.p. 100–102 °C; R_f 0.35 (2 : 8, EtOAc/hexane v/v); ^1H NMR (500 MHz, CDCl_3): δ = 8.75 (d, J = 9.3 Hz, 1H), 8.43 (s, 1H), 8.22 (d, J = 8.2 Hz, 1H), 8.12 (d, J = 8.0 Hz, 2H), 7.77 (t, J = 8.0 Hz, 1H), 7.64–7.61 (m, 1H), 7.35 (d, J = 6.9 Hz, 2H), 5.08 (d, J = 2.7 Hz, 2H), 2.60 (t, J = 2.7 Hz, 1H), 2.45 (s, 3H); ^{13}C NMR (125 MHz, CDCl_3): δ = 165.74, 156.85, 149.45, 140.15, 136.08, 134.79, 130.47, 130.08, 129.84, 127.93, 127.53, 125.43, 123.95, 120.56, 77.03, 75.82, 53.22, 21.51; HRMS (ESI): m/z calculated for $\text{C}_{20}\text{H}_{16}\text{NO}_2$, $[\text{M} + \text{H}]^+$ 302.1103, found 302.1162.

2.4. General experimental procedure for the synthesis of 1,2,3-triazole linked quinoline glycoconjugates 6(a–k)

A solution of prop-2-yn-1-yl 2-phenylquinoline-4-carboxylate (**4a**; 1.0 equiv.), 2,3,4,6-tetra-*O*-acetyl- β -D-glucopyranosyl azide and (**5a**; 1.0 equiv.), was prepared in dichloromethane. To this reaction mixture, *N,N*-diisopropylethylamine (DIPEA; 0.5 equiv.) and copper iodide (CuI; 0.3 equiv.) were added with continuous stirring at room temperature. The reaction mixture was stirred at room temperature for 6 h, and the progress was monitored by TLC using 50% ethyl acetate in hexane. Visualization of TLC was performed by charring with 5% concentrated H_2SO_4 in methanol. After completion, the solvent was evaporated under reduced pressure, and the crude product was subsequently purified by column chromatography. Other derivatives (**6b–6k**) were synthesized following the same general procedure.

2.4.1. 1-(2,3,4,6-Tetra-*O*-acetyl- β -D-glucopyranosyl)-1H-1,2,3-triazole-4-yl)methyl-2-phenylquinoline-4-carboxylate (6a). A solution of **4a** (0.250 g, 0.870 mmol), 2,3,4,6-tetra-*O*-acetyl- β -D-glucopyranosyl azide (**5a**; 0.324 g, 0.870 mmol), CuI (0.049 g, 0.261 mmol) and DIPEA (0.075 mL, 0.435 mmol), was prepared in 4 mL dichloromethane and reacted as described above. After chromatographic purification obtained **6a**. White crystalline powder; yield 0.454 g (79%); m.p. 165–167 °C; R_f 0.30 (3 : 7, EtOAc : hexane, v/v); IR (ν cm^{-1} , KBr) 1460C=N, 1598 C=C, 1745 (–O{CO}), 2923, 3095; ^1H NMR (500 MHz, CDCl_3): δ 8.73 (d, J = 9.3 Hz, 1H), 8.40 (s, 1H), 8.20 (dd, J = 13.3, 8.0 Hz, 3H), 8.03 (s, 1H), 7.76 (t, J = 7.3 Hz, 1H), 7.63 (t, J = 8.0 Hz, 1H), 7.52 (t, J = 7.3 Hz, 2H), 7.49–7.45 (m, 1H), 5.91–5.88 (m, 1H), 5.62 (s, 2H), 5.45–5.41 (m, 2H), 5.26–5.21 (m, 1H), 4.30 (dd, J = 12.7, 4.7 Hz, 1H), 4.15 (d, J = 12.0 Hz, 1H), 4.03–3.99 (m, 1H), 2.06 (s, 3H), 2.05 (s, 3H), 2.02 (s, 3H), 1.82 (s, 3H). ^{13}C NMR (125 MHz, CDCl_3): δ = 170.58, 169.99, 169.46, 168.96, 166.29, 156.88, 149.40, 143.31, 138.84, 135.27, 130.49, 130.09, 129.89, 129.04, 128.06, 127.66, 125.48, 124.07, 122.87, 120.69, 86.06, 75.45, 72.63, 70.57, 67.83, 61.62, 58.60, 20.77, 20.63, 20.20; HRMS



(ESI): m/z calculated for $C_{33}H_{33}N_4O_{11}$, $[M + H]^+$ 661.2068, found 661.2141.

2.4.2. 1-(2,3,4,6-Tetra-O-acetyl- β -D-glucopyranosyl)-1H-1,2,3-triazole-4-yl)methyl-2-(4-chlorophenyl) quinoline-4-carboxylate (6b). A solution of prop-2-yn-1-yl 2(4-chlorophenyl)quinoline-4-carboxylate **4b** (0.300 g, 0.932 mmol), **5a** (0.347 g, 0.932 mmol), CuI (0.053 g, 0.279 mmol) and DIPEA (0.081 mL, 0.466 mmol), was prepared in 4 mL dichloromethane and reacted as described above. After chromatographic purification **6b** was obtained. Light yellow powder; yield 0.531 g (82%); m.p. 163–165 °C; R_f 0.35 (3 : 7, EtOAc : hexane, v/v); IR (ν cm^{-1} , KBr) 1547C=N, 1596 C=C, 1732 (–O{CO}), 2976, 3117; 1H NMR (600 MHz, $CDCl_3$): δ = 8.73 (d, J = 7.6 Hz, 1H), 8.36 (s, 1H), 8.18 (d, J = 8.2 Hz, 1H), 8.16–8.14 (m, 2H), 8.03 (s, 1H), 7.76 (ddd, J = 8.4, 6.8, 1.4 Hz, 1H), 7.63 (ddd, J = 8.3, 6.8, 1.3 Hz, 1H), 7.49–7.47 (m, 2H), 5.91–5.89 (m, 1H), 5.62 (s, 2H), 5.43–5.42 (m, 2H), 5.24 (ddd, J = 9.7, 6.4, 2.8 Hz, 1H), 4.30 (dd, J = 12.6, 5.0 Hz, 1H), 4.15 (dd, J = 12.7, 2.1 Hz, 1H), 4.01 (ddd, J = 10.2, 5.0, 2.2 Hz, 1H), 2.05 (s, 6H), 2.02 (s, 3H), 1.83 (s, 3H); ^{13}C NMR (150 MHz, $CDCl_3$): δ = 170.55, 169.98, 169.45, 168.98, 166.11, 155.47, 149.32, 143.22, 137.16, 136.15, 135.38, 130.44, 130.25, 129.22, 128.89, 128.26, 125.50, 124.09, 122.87, 120.19, 86.04, 75.44, 72.59, 70.55, 67.79, 61.59, 58.62, 20.78, 20.65, 20.62, 20.23; HRMS (ESI): m/z calculated for $C_{33}H_{32}ClN_4O_{11}$, $[M + H]^+$ 695.1678, found 695.1763.

2.4.3. 1-(2,3,4,6-Tetra-O-acetyl- β -D-glucopyranosyl)-1H-1,2,3-triazole-4-yl)methyl-2-(4-methoxyphenyl) quinoline-4-carboxylate (6c). A solution of prop-2-yn-1-yl 2(4-methoxyphenyl)quinoline-4-carboxylate **4c** (0.350 g, 1.10 mmol), **5a** (0.411 g, 1.10 mmol), CuI (0.063 g, 0.330 mmol) and DIPEA (0.096 mL, 0.551 mmol), was prepared in 4 mL dichloromethane and reacted as described above. After chromatographic purification **6c** was obtained. White powder; yield 0.624 g (82%); m.p. 170–172 °C; R_f 0.40 (3 : 7, EtOAc : hexane, v/v); IR (ν cm^{-1} , KBr) 1589C=N, 1604 C=C, 1754 (–O{CO}), 2922, 3138; 1H NMR (500 MHz, $CDCl_3$): δ = 8.69 (d, J = 8.5 Hz, 1H), 8.36 (s, 1H), 8.16 (d, J = 8.9 Hz, 3H), 8.03 (s, 1H), 7.73 (t, J = 6.9 Hz, 1H), 7.58 (t, J = 7.0 Hz, 1H), 7.03 (d, J = 8.8 Hz, 2H), 5.93–5.87 (m, 1H), 5.62 (s, 2H), 5.47–5.39 (m, 2H), 5.24 (t, J = 9.7 Hz, 1H), 4.30 (dd, J = 12.6, 5.0 Hz, 1H), 4.15 (d, J = 12.6 Hz, 1H), 4.01 (td, J = 4.9, 2.7 Hz, 1H), 3.87 (s, 3H), 2.05 (d, J = 5.0 Hz, 6H), 2.02 (s, 3H), 1.82 (s, 3H); ^{13}C NMR (125 MHz, $CDCl_3$): δ = 170.57, 169.99, 169.44, 168.94, 166.34, 161.28, 156.36, 149.35, 143.30, 135.06, 131.36, 130.23, 129.98, 129.01, 127.61, 125.42, 123.70, 122.88, 120.25, 114.41, 86.01, 75.40, 72.61, 70.51, 67.78, 61.59, 58.54, 55.52, 20.77, 20.63, 20.61, 20.21; HRMS (ESI): m/z calculated for $C_{34}H_{35}N_4O_{12}$, $[M + H]^+$ 691.2173, found 691.2230.

2.4.4. 1-(2,3,4,6-Tetra-O-acetyl- β -D-glucopyranosyl)-1H-1,2,3-triazole-4-yl)methyl-2-(4-fluorophenyl) quinoline-4-carboxylate (6d). A solution of prop-2-yn-1-yl 2(4-fluorophenyl)quinoline-4-carboxylate (**4d**; 0.300 g, 0.982 mmol), **5a** (0.366 g, 0.982 mmol), CuI (0.056 g, 0.294 mmol) and DIPEA (0.085 mL, 0.491 mmol), was prepared in 4 mL dichloromethane and reacted as described above. After chromatographic purification **6d** obtained. White cream powder; yield 0.546 g (82%); m.p. 161–163 °C; R_f 0.35 (3 : 7, EtOAc : hexane, v/v); IR (ν cm^{-1} , KBr) 1588C=N, 1600C=C, 1755 (–O{CO}), 2924, 3098; 1H NMR (600

MHz, $CDCl_3$): δ 8.72 (dd, J = 16.8, 8.8 Hz, 1H), 8.37 (s, 1H), 8.22–8.15 (m, 3H), 8.02 (s, 1H), 7.75 (dt, J = 15.5, 7.9 Hz, 1H), 7.61 (dt, J = 21.5, 7.9 Hz, 1H), 7.22–7.18 (m, 1H), 7.03 (d, J = 8.2 Hz, 1H), 5.62 (s, 2H), 5.43 (d, J = 8.0 Hz, 2H), 5.24 (t, J = 6.8 Hz, 1H), 4.31 (dd, J = 12.6, 4.8 Hz, 1H), 4.14 (dd, J = 18.1, 10.0 Hz, 2H), 4.01 (dd, J = 10.3, 5.0 Hz, 1H). ^{13}C NMR (150 MHz, $CDCl_3$): δ = 171.82, 170.08, 169.45, 168.98, 166.22, 160.74, 155.75, 149.76, 143.28, 135.10, 130.43, 130.29, 129.99, 129.57, 129.04, 128.13, 127.61, 125.52, 122.85, 120.28, 116.12, 115.0, 86.10, 75.50, 72.66, 70.60, 67.86, 61.64, 58.64, 20.78, 20.63, 20.22; HRMS (ESI): m/z calculated for $C_{33}H_{32}FN_4O_{11}$, $[M + H]^+$ 679.1973, found 679.2066.

2.4.5. 1-(2,3,4,6-Tetra-O-acetyl- β -D-glucopyranosyl)-1H-1,2,3-triazole-4-yl)methyl-2-(4-methylphenyl)quinoline-4-carboxylate (6e). A solution of prop-2-yn-1-yl 2(4-methylphenyl)quinoline-4-carboxylate (**4e**; 0.250 g, 0.830 mmol), **5a** (0.309 g, 0.830 mmol), CuI (0.047 g, 0.249 mmol) and DIPEA (0.072 mL, 0.415 mmol), was prepared in 4 mL dichloromethane and reacted as described above. After chromatographic purification **6e** was obtained. White powder; yield 0.453 g (81%); m.p. 166–168 °C; R_f 0.30 (3 : 7, EtOAc : hexane, v/v); IR (ν cm^{-1} , KBr) 1493C=N, 1596C=C, 1749 (–O{CO}), 2922, 3064; 1H NMR (600 MHz, $CDCl_3$): δ = 8.71 (d, J = 9.8 Hz, 1H), 8.39 (s, 1H), 8.19 (d, J = 7.6 Hz, 1H), 8.10 (d, J = 8.2 Hz, 2H), 8.03 (s, 1H), 7.75 (t, J = 6.9 Hz, 1H), 7.60 (t, J = 7.7 Hz, 1H), 7.32 (d, J = 8.1 Hz, 2H), 5.90–5.88 (m, 1H), 5.62 (s, 2H), 5.44–5.42 (m, 2H), 5.26–5.22 (m, 1H), 4.30 (dd, J = 12.6, 5.0 Hz, 1H), 4.15 (dd, J = 12.6, 2.2 Hz, 1H), 4.02–3.99 (m, 1H), 2.43 (s, 3H), 2.06 (d, J = 4.5 Hz, 6H), 2.02 (s, 3H), 1.83 (s, 3H); ^{13}C NMR (150 MHz, $CDCl_3$): δ = 170.58, 169.99, 169.44, 168.94, 166.34, 156.79, 149.37, 143.32, 140.08, 136.01, 135.11, 130.40, 130.00, 129.77, 127.83, 127.50, 125.44, 123.93, 122.87, 120.51, 86.03, 75.42, 72.62, 70.52, 67.79, 61.59, 58.57, 21.49, 20.79, 20.65, 20.62, 20.22; HRMS (ESI): m/z calculated for $C_{33}H_{35}N_4O_{11}$, $[M + H]^+$ 675.2224, found 675.2290.

2.4.6. 1-(2,3,4,6-Tetra-O-acetyl- β -D-galactopyranosyl)-1H-1,2,3-triazole-4-yl)methyl-2-phenylquinoline-4-carboxylate (6f). A solution of **4a** (0.250 g, 0.870 mmol), 2,3,4,6-Tetra-O-acetyl- β -D-galactopyranosyl azide (**5b**; 0.324 g, 0.870 mmol), CuI (0.049 g, 0.261 mmol) and DIPEA (0.075 mL, 0.435 mmol), was prepared in 4 mL dichloromethane and reacted as described above. After chromatographic purification **6f** was obtained. White powder; yield 0.459 g (80%); m.p. 160–162 °C; R_f 0.30 (3 : 7, EtOAc : hexane, v/v); IR (ν cm^{-1} , KBr) 1495C=N, 1549 C=C, 1755 (–O{CO}), 2925, 3472; 1H NMR (500 MHz, $CDCl_3$): δ = 8.73 (d, J = 9.3 Hz, 1H), 8.41 (s, 1H), 8.21 (dd, J = 12.0, 8.0 Hz, 3H), 8.08 (s, 1H), 7.77 (t, J = 8.0 Hz, 1H), 7.63 (t, J = 7.3 Hz, 1H), 7.54–7.48 (m, 2H), 7.46 (d, J = 8.0 Hz, 1H), 5.86 (d, J = 9.3 Hz, 1H), 5.63 (s, 2H), 5.55–5.53 (m, 2H), 5.26 (dd, J = 10.0, 4.7 Hz, 1H), 4.24–4.20 (m, 1H), 4.18 (q, J = 4.0 Hz, 1H), 4.14 (dd, J = 12.0, 6.7 Hz, 1H), 2.20 (s, 3H), 2.01 (d, J = 10.7 Hz, 6H), 1.85 (s, 3H); ^{13}C NMR (125 MHz, $CDCl_3$): δ = 170.42, 170.08, 169.88, 169.12, 166.34, 156.86, 149.41, 143.21, 138.83, 135.33, 130.52, 130.10, 129.90, 129.05, 128.04, 127.64, 125.46, 124.05, 123.00, 120.66, 86.60, 74.37, 70.79, 68.16, 66.96, 61.29, 58.59, 20.77, 20.72, 20.58, 20.29; HRMS (ESI): m/z calculated for $C_{33}H_{32}N_4O_{11}$, $[M + H]^+$ 661.2068, found 661.2141.



2.4.7. 1-(2,3,4,6-Tetra-O-acetyl-β-D-galactopyranosyl)-1H-1,2,3-triazole-4-yl)methyl-2-(4-chlorophenyl) quinoline-4-carboxylate (6g). A solution of **4b** (0.300 g, 0.932 mmol), **5b** (0.347 g, 0.932 mmol), CuI (0.053 g, 0.279 mmol) and DIPEA (0.081 mL, 0.466 mmol), was prepared in 4 mL dichloromethane and reacted as described above. After chromatographic purification **6g** was obtained. Yellowish powder; yield 0.537 g (83%); m.p. 161–163 °C; R_f 0.35 (3 : 7, EtOAc : hexane, v/v); IR (ν cm⁻¹, KBr) 1575 C=N, 1627 C=C, 1755 (-O{CO}), 2926, 3328; ¹H NMR (600 MHz, DMSO-*d*₆): δ = 8.61 (d, J = 8.4 Hz, 1H), 8.36 (s, 1H), 8.29 (s, 1H), 8.19 (d, J = 8.2 Hz, 2H), 8.10 (d, J = 8.4 Hz, 1H), 7.94 (s, 1H), 7.76 (t, J = 7.6 Hz, 1H), 7.61 (t, J = 7.6 Hz, 1H), 7.47 (d, J = 8.2 Hz, 2H), 6.21 (d, J = 9.1 Hz, 1H), 5.54 (dd, J = 21.4, 8.1 Hz, 2H), 5.43 (s, 2H), 4.53 (t, J = 6.4 Hz, 1H), 4.11 (dd, J = 11.6, 5.6 Hz, 1H), 4.02 (dd, J = 11.4, 6.9 Hz, 1H), 3.36 (ddd, J = 10.5, 7.3, 3.8 Hz, 1H), 2.13 (s, 3H), 1.93 (d, J = 11.8 Hz, 6H), 1.76 (s, 3H); ¹³C NMR (150 MHz, DMSO-*d*₆): δ = 168.34, 167.87, 167.06, 164.05, 155.80, 153.32, 147.31, 140.87, 135.30, 134.27, 134.09, 128.78, 128.62, 127.50, 127.37, 126.64, 123.83, 122.44, 122.18, 118.08, 83.56, 71.80, 69.00, 66.72, 65.83, 59.92, 57.13, 19.13, 19.07, 19.00, 18.69; HRMS (ESI): m/z calculated for C₃₃H₃₂ClN₄O₁₁, [M + H]⁺ 695.1678, found 695.1759.

2.4.8. 1-(2,3,4,6-Tetra-O-acetyl-β-D-galactopyranosyl)-1H-1,2,3-triazole-4-yl)methyl-2-(4-methoxyphenyl) quinoline-4-carboxylate (6h). A solution of **4c** (0.350 g, 1.10 mmol), **5b** (0.411 g, 1.10 mmol), CuI (0.063 g, 0.330 mmol) and DIPEA (0.096 mL, 0.551 mmol), was prepared in 4 mL dichloromethane and reacted as described above. After chromatographic purification **6h** was obtained. Cream colour powder; yield 0.608 g (80%); m.p. 164–166 °C; R_f 0.35 (3 : 7, EtOAc : hexane, v/v); IR (ν cm⁻¹, KBr) 1591 C=N, 1605 C=C, 1747 (-O{CO}), 2966, 3134; ¹H NMR (500 MHz, CDCl₃): δ = 8.70 (d, J = 9.4 Hz, 1H), 8.36 (s, 1H), 8.17 (d, J = 8.9 Hz, 3H), 8.08 (s, 1H), 7.75–7.73 (m, 1H), 7.60–7.57 (m, 1H), 7.03 (d, J = 8.9 Hz, 2H), 5.86 (d, J = 9.4 Hz, 1H), 5.63 (s, 2H), 5.55–5.53 (m, 2H), 5.25 (dd, J = 10.4, 3.4 Hz, 1H), 4.24–4.12 (m, 3H), 3.88 (s, 3H), 2.20 (s, 3H), 2.02 (s, 3H), 2.00 (s, 3H), 1.85 (s, 3H); ¹³C NMR (125 MHz, CDCl₃): δ = 170.42, 170.08, 169.89, 169.12, 166.41, 161.29, 156.38, 149.37, 143.22, 135.15, 131.37, 130.26, 130.00, 129.01, 127.61, 125.41, 123.70, 123.02, 120.24, 114.42, 86.56, 74.33, 70.77, 68.11, 66.93, 61.29, 58.54, 20.78, 20.74, 20.60, 20.32; HRMS (ESI): m/z calculated for C₃₄H₃₅N₄O₁₂, [M + H]⁺ 691.2173, found 691.2224.

2.4.9. 1-(2,3,4,6-Tetra-O-acetyl-β-D-galactopyranosyl)-1H-1,2,3-triazole-4-yl)methyl-2-(4-fluorophenyl) quinoline-4-carboxylate (6i). A solution of **4d** (0.300 g, 982 μmol), **5b** (0.366 g, 0.982 mmol), CuI (0.056 g, 0.294 mmol) and DIPEA (0.085 mL, 0.491 mmol), was prepared in 4 mL dichloromethane and reacted as described above. After chromatographic purification **6i** was obtained. White powder; yield 0.540 g (81%); m.p. 163–165 °C; R_f 0.30 (3 : 7, EtOAc : hexane, v/v); IR (ν cm⁻¹, KBr) 1503 C=N, 1592 C=C, 1750 (-O{CO}), 2926, 3489; ¹H NMR (600 MHz, CDCl₃): δ = 8.72 (d, J = 8.0 Hz, 1H), 8.36 (s, 1H), 8.21–8.18 (m, 2H), 8.08 (s, 1H), 7.76 (t, J = 8.0 Hz, 1H), 7.64–7.61 (m, 1H), 7.20 (t, J = 8.7 Hz, 2H), 7.02 (d, J =

9.3 Hz, 1H), 5.87 (d, J = 9.3 Hz, 1H), 5.63 (s, 2H), 5.55–5.53 (m, 2H), 5.26 (dd, J = 10.7, 4.0 Hz, 1H), 4.22–4.13 (m, 3H), 2.20 (s, 3H), 2.02 (s, 3H), 2.00 (s, 3H), 1.85 (s, 3H); ¹³C NMR (150 MHz, CDCl₃): δ = 170.39, 170.04, 169.86, 169.14, 166.23, 155.69, 149.36, 143.17, 135.45, 130.41, 130.20, 129.6, 129.53, 129.0, 128.08, 125.48, 123.96, 122.97, 120.23, 116.08, 115.91, 114.96, 86.6, 74.39, 70.78, 68.19, 66.96, 61.30, 58.61, 20.74, 20.70, 20.57, 20.29; HRMS (ESI): m/z calculated for C₃₃H₃₂FN₄O₁₁, [M + H]⁺ 679.1973, found 679.2020.

2.4.10. 1-(2,3,4,6-Tetra-O-acetyl-β-D-galactopyranosyl)-1H-1,2,3-triazole-4-yl)methyl-2-(4-methylphenyl) quinoline-4-carboxylate (6j). A solution of **4e** (0.250 g, 0.830 mmol), **5b** (0.309 g, 0.830 mmol), CuI (0.047 g, 0.249 mmol) and DIPEA (0.072 mL, 0.415 mmol), was prepared in 4 mL dichloromethane and reacted as described above. After chromatographic purification **6j** was obtained. White powder; yield 0.447 g (80%); m.p. 161–163 °C; R_f 0.30 (3 : 7, EtOAc : hexane, v/v); IR (ν cm⁻¹, KBr) 1548 C=N, 1593 C=C, 1755 (-O{CO}), 2923, 3492; ¹H NMR (600 MHz, CDCl₃): δ = 8.71 (d, J = 10.1 Hz, 1H), 8.39 (s, 1H), 8.20 (d, J = 9.8 Hz, 1H), 8.10 (d, J = 8.2 Hz, 2H), 8.07 (s, 1H), 7.75 (t, J = 8.4 Hz, 1H), 7.61 (t, J = 8.4 Hz, 1H), 7.32 (d, J = 8.0 Hz, 2H), 5.86 (d, J = 9.4 Hz, 1H), 5.63 (s, 2H), 5.55–5.53 (m, 2H), 5.26 (dd, J = 10.4, 3.4 Hz, 1H), 4.23–4.12 (m, 3H), 2.43 (s, 3H), 2.20 (s, 3H), 2.02 (s, 3H), 2.00 (s, 3H), 1.85 (s, 3H); ¹³C NMR (150 MHz, CDCl₃): δ = 170.42, 170.09, 169.89, 169.12, 166.41, 156.78, 149.36, 143.21, 140.08, 135.99, 135.19, 130.37, 130.01, 129.77, 127.81, 127.49, 125.41, 123.91, 123.03, 120.49, 86.56, 74.33, 70.77, 68.11, 66.93, 61.29, 58.55, 21.49, 20.78, 20.74, 20.60, 20.31; HRMS (ESI): m/z calculated for C₃₃H₃₅N₄O₁₁, [M + H]⁺ 675.2224, found 675.2323.

2.4.11. 1-(5-Deoxy-1,2-O-isopropylidene-α-D-xylofuranose-5-yl)-1H-1,2,3-triazol-4-yl)methyl-2-phenylquinoline-4-carboxylate (6k). A solution of **4a** (0.200 g, 0.69 mmol), 5-azido-5-deoxy-1,2-O-isopropylidene-α-D-xylofuranose²² (**5c**; 0.150 g, 0.69 mmol), CuI (0.040 g, 0.21 mmol) and DIPEA (60 μL, 0.34 mmol), was prepared in 4 mL dichloromethane and reacted as described above. After chromatographic purification **6k** was obtained. Light creamy powder; yield 0.284 g (81%); m.p. 155–158 °C; R_f 0.35 (3 : 7, EtOAc : hexane, v/v); ¹H NMR (500 MHz, CDCl₃) δ 8.74 (d, J = 9.3 Hz, 1H), 8.40 (s, 1H), 8.21 (d, J = 8.0 Hz, 1H), 8.16 (d, J = 6.7 Hz, 2H), 7.90 (s, 1H), 7.76 (t, J = 7.3 Hz, 1H), 7.62 (t, J = 8.0 Hz, 1H), 7.53 (t, J = 7.3 Hz, 2H), 7.47 (t, J = 6.7 Hz, 1H), 5.96 (d, J = 4.0 Hz, 1H), 5.66–5.56 (m, 2H), 4.79 (dd, J = 13.3, 6.7 Hz, 1H), 4.64–4.52 (m, 2H), 4.47 (t, J = 6.7 Hz, 1H), 4.23 (s, 1H), 3.49 (d, J = 5.3 Hz, 1H), 1.41 (s, 3H), 1.27 (s, 3H). ¹³C NMR (125 MHz, CDCl₃) δ 166.29, 156.93, 149.34, 142.55, 138.78, 135.19, 130.42, 130.15, 129.93, 129.09, 128.11, 127.67, 125.75, 125.43, 124.07, 120.75, 112.24, 105.26, 85.39, 79.20, 74.76, 58.69, 48.86, 26.89, 26.24. HRMS (ESI): m/z calculated for C₂₂H₂₆N₄O₆, [M + H]⁺ 503.1852, found 503.1884.

2.5. Cell culture

The MCF-7 human breast cancer cell line was obtained from the National Centre for Cell Science (NCCS), Pune, India. The cells were maintained in Dulbecco's Modified Eagle's Medium (DMEM) enriched with 10% fetal bovine serum (FBS) and 100 U



mL^{-1} penicillin–streptomycin, under standard culture conditions of 37 °C in a humidified atmosphere containing 5% CO_2 . Stock solutions of the synthesized compounds **6(a–j)** were initially prepared in dimethyl sulfoxide (DMSO) and subsequently diluted with complete medium to achieve the required test concentrations. The final concentration of DMSO in all experimental treatments was kept below 0.1% (v/v) to avoid solvent-related cytotoxic effects.

2.6. Cell viability assay

The cytotoxic activity of the synthesized compounds **6(a–j)** was evaluated against MCF-7 human breast cancer cells using the MTT colorimetric assay. In brief, cells were seeded into 96-well culture plates and incubated for 48 hours under standard growth conditions (37 °C, 5% CO_2 , and a humidified atmosphere) to achieve approximately 70% confluence. After cell attachment, the medium was replaced with fresh DMEM containing various concentrations of the test compounds (50–200 $\mu\text{g mL}^{-1}$), followed by an additional 48-hours incubation. Post-treatment, the medium was replaced with 200 μL of serum-free DMEM containing 20 μL of MTT solution (5 mg mL^{-1}) and incubated for 4 hours to facilitate formazan crystal formation. The resulting supernatant was carefully removed, and the formazan precipitate was dissolved in 100 μL of DMSO. The absorbance of each well was recorded at 590 nm using a microplate reader, and the cell viability was calculated relative to the untreated control group.

$$\% \text{ Of cell survival} = \left(\frac{\text{mean O. D. of the drug treated well}}{\text{mean O.D. of the control well}} \right) \times 100.$$

2.7. Molecular docking study

The crystal structure of the human oestrogen receptor alpha ($\text{ER}\alpha$) complexed with the inhibitor 4-hydroxy tamoxifen (PDB ID: 3ERT) was obtained from RCSB Protein Data Bank (<https://www.rcsb.org>). Molecular docking simulations were performed using AutoDock vina 4.2 to examine the interaction between the ligand and the receptor.^{23,24} Using the Gaussian09W software

package, geometry optimisations were carried out at the B3LYP/6-31G(d,p) level of theory to determine the structures of compounds **6(a–j)**. The ligand–protein interactions were analysed and visualised in both 2D and 3D formats using BIOVIA Discovery Studio Visualiser.

2.8. Crystallography

Single clear white needle-shaped crystals of **6a**, **6b** and **6e** were obtained by recrystallisation from ethyl acetate and chloroform layering. A suitable crystal $0.03 \times 0.02 \times 0.01$ mm was selected and mounted on a suitable support on an XtaLAB Synergy, Dualflex, HyPix3000 diffractometer. The crystal was kept at a steady $T = 293$ K during data collection. The structure was solved with the ShelXT 2018/2.²⁵ Structure solution program using the Intrinsic phasing solution method and by using Olex2 as the graphical interface.²⁶ The model was refined with version 2019/2 of ShelXL 2019/2 using Least Squares minimisation.²⁷

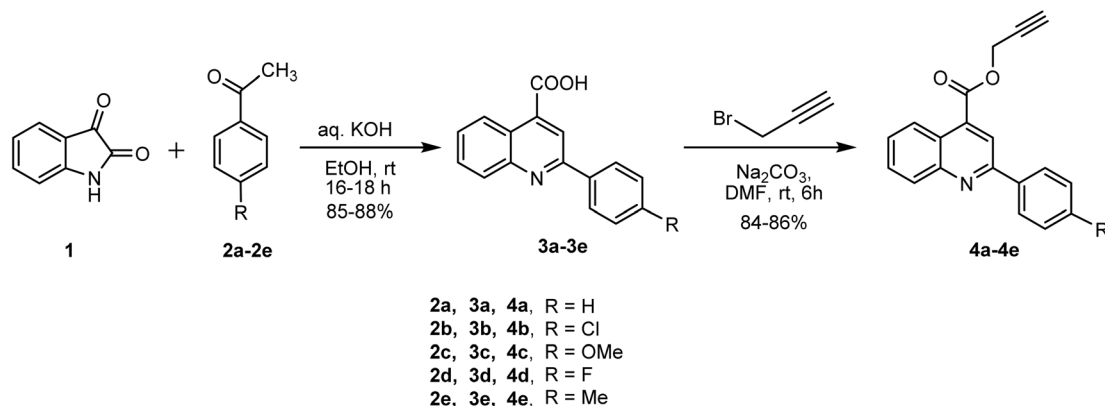
2.9. DFT studies

All DFT calculations in the present study were carried out using the Gaussian 09W software package.²⁸ The visualization and interpretation of the optimized geometries and electronic properties were performed using GaussView 5.0.²⁹ Initially, all molecular geometries were optimized in the gas phase without imposing any symmetry constraints. The calculations were conducted at the density functional theory (DFT) level employing the B3LYP functional. The B3LYP method combines Becke's three-parameter hybrid exchange functional (B3) with the Lee–Yang–Parr (LYP) correlation functional, providing a reliable balance between computational efficiency and accuracy.³⁰ This functional effectively incorporates both local and non-local electron correlation effects, making it widely suitable for studying molecular geometries, electronic structures, and reactivity parameters.

3. Result and discussion

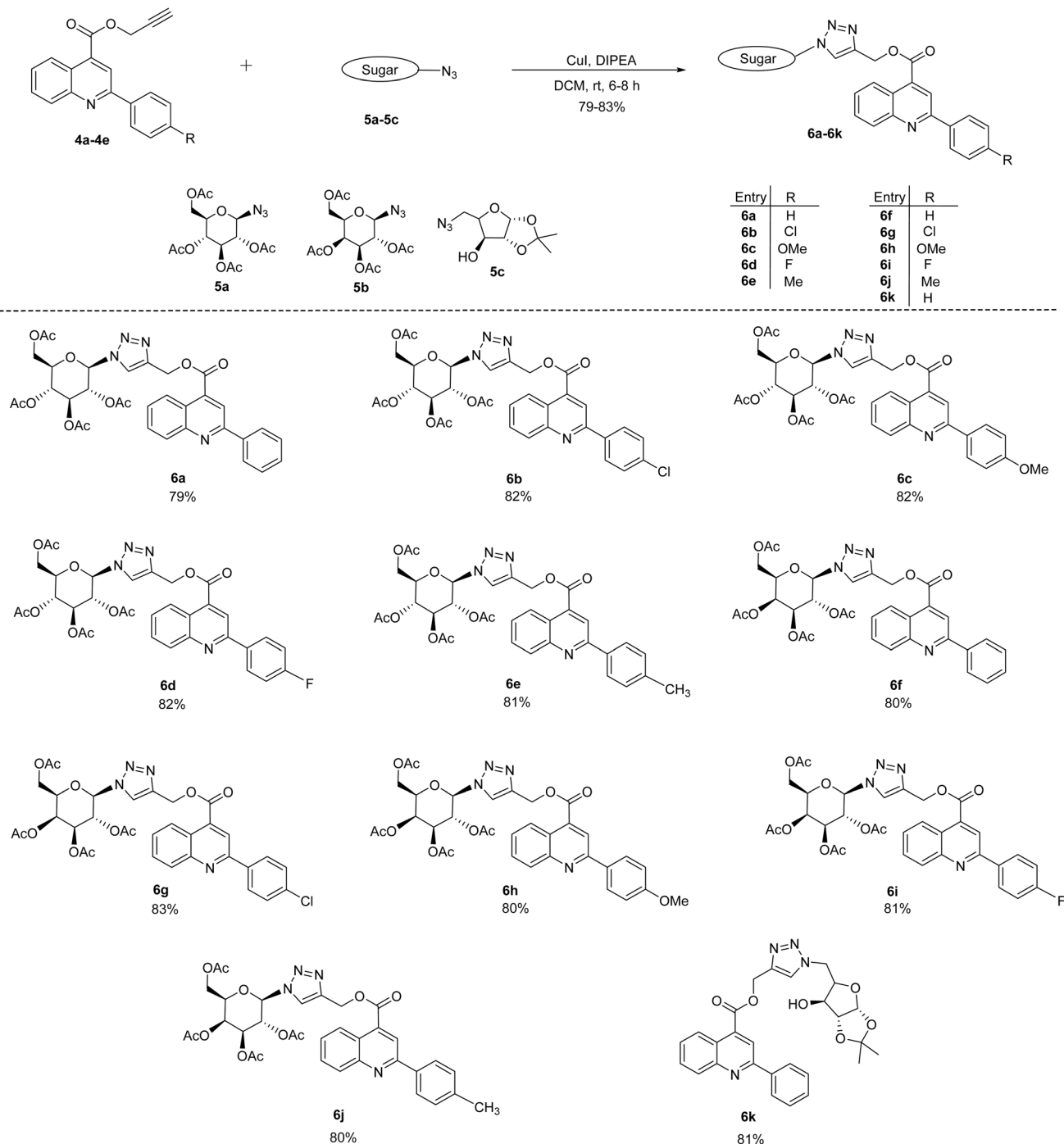
3.1. Synthesis

Quinoline-4-carboxylic acids and their derivatives are important building blocks for various pharmaceuticals and other



Scheme 1 Synthesis of prop-2-yn-1-yl 2-phenylquinoline-4-carboxylate derivatives (**4a–4e**).





Scheme 2 Synthesis of 1,2,3- triazole linked quinoline glycoconjugates 6(a–k).

biologically active compounds. The Pfitzinger reaction is a versatile and efficient method for the synthesis of quinoline-4-carboxylic acids, but it can be challenging to achieve high yields and good purity.²¹ In this study, the Pfitzinger reaction was successfully employed to synthesize a series of 2-phenylquinoline-4-carboxylic acids 3(a–e) from isatin and substituted acetophenones under mild conditions, affording excellent yields (85–88%). The reactions were carried out in ethanol using an aqueous KOH under reflux conditions, and the

products were isolated by simple filtration followed by recrystallization.

The structure of compound 3a was confirmed by spectroscopic analysis. Its IR spectrum showed characteristic absorption bands at 3400–3300 cm^{-1} corresponding to O–H stretching and at 1670–1700 cm^{-1} attributed to C=O stretching of the carboxylic acid group. In the ^{13}C NMR spectrum, a signal at δ 168.27 ppm was assigned to the carboxylic acid carbon. Further confirmation was done by the HRMS analysis, which



Table 1 Cell viability and IC₅₀ value of compounds 6(a–j) against MCF-7 cell line

| Compound no. | Cell viability % ± SD | | | IC ₅₀ (μM) |
|--------------|--------------------------------------|---------------|--------------|-----------------------|
| | Concentration (μg mL ⁻¹) | | | |
| | 50 | 100 | 200 | |
| 6a | 70.74 ± 2.10 | 66.61 ± 2.19 | 50.18 ± 0.85 | >200 |
| 6b | 99.46 ± 0.70 | 81.93 ± 2.12 | 79.79 ± 1.41 | >200 |
| 6c | 50.46 ± 0.32 | 54.30 ± 0.88 | 43.47 ± 3.40 | 131.25 |
| 6d | 63.57 ± 0.93 | 50.96 ± 1.23 | 48.56 ± 2.67 | 135.95 |
| 6e | 57.41 ± 0.70 | 57.83 ± 0.70 | 50.49 ± 0.21 | >200 |
| 6f | 75.15 ± 12.39 | 50.28 ± 7.10 | 27.98 ± 1.23 | 108.59 |
| 6g | 79.76 ± 0.70 | 64.61 ± 1.41 | 50.90 ± 0.70 | >200 |
| 6h | 52.60 ± 2.59 | 50.40 ± 11.20 | 58.59 ± 3.80 | >200 |
| 6i | 55.92 ± 0.70 | 51.10 ± 1.22 | 22.68 ± 1.52 | 151.36 |
| 6j | 72.37 ± 8.59 | 54.95 ± 3.68 | 49.95 ± 1.22 | 198.61 |
| Tamoxifen | — | — | — | 22 |

showed a molecular ion peak at m/z 250.0837 $[M + H]^+$, consistent with the molecular formula C₁₆H₁₂NO₂. Similar spectroscopic features confirmed structure of remaining compounds 3(b–e).

Subsequently, compounds 3(a–e) were subjected to propargylation using propargyl bromide in the presence of potassium carbonate in DMF at room temperature. This reaction furnished the corresponding prop-2-yn-1-yl 2-phenylquinoline-4-carboxylate derivatives 4(a–e) in good yields (84–86%) (Scheme 1). The successful formation of the propargylated products was confirmed by NMR and HRMS analyses. The ¹H NMR spectra of compound 4a displayed peak at δ 2.60 ppm corresponding to the acetylenic proton ($\equiv CH$) and a doublet at δ 5.07 ppm assigned to methylene protons ($-OCH_2-$). In the ¹³C NMR spectrum, signals observed at approximately δ 75 ppm corresponded to acetylenic carbon ($C\equiv CH$), and the signal at δ 53.25 ppm was resonated for the methylene carbon ($-OCH_2-$). HRMS spectrum further supported the structure of compound 4a, showing a molecular ion peak at m/z 288.1012 $[M + H]^+$, in agreement with the molecular formula C₁₉H₁₄NO₂.

Next, glycopyranosyl azides 5a and 5b were synthesized starting from D-glucose and D-galactose, respectively. The sugars were first peracetylated using acetic anhydride in pyridine to afford the corresponding per-O-acetylated glycopyranosides, which were then converted to 2,3,4,6-tetra-O-acetyl- α -D-glycopyranosyl bromides using 33% HBr in glacial acetic acid at 0 °C to room temperature in dry dichloromethane. Subsequently, these intermediates were reacted with sodium azide in DMSO at room temperature, furnishing 2,3,4,6-tetra-O-acetyl- β -D-glycopyranosyl azides 5a and 5b in excellent yields. 5-Azido-5-deoxy-1,2-O-isopropylidene- α -D-xylofuranose (5c) was synthesized from the D-xylose using a series of reactions according to reported method.²²

A Cu(I) catalyzed azide-alkyne cycloaddition reaction was performed between quinoline-derived alkynes (4a–4e) and glycopyranosyl azides (5a, 5b and 5c) in dichloromethane using catalytic amount of CuI and *N,N*-diisopropylethylamine at room temperature (Scheme 2). This reaction afforded the desired 1,4-disubstituted 1,2,3-triazole-linked 2-phenylquinoline-4-

carboxylate derivatives 6(a–k) in 79–83% yield. The structures of compounds 6(a–k) were confirmed by IR, ¹H & ¹³C NMR spectroscopy and HRMS analyses. The ¹H NMR spectrum of compound 6a showed a characteristic singlet corresponding to triazolyl proton at δ 8.03 ppm, whereas two methylene ($-CH_2-$) protons attached to the triazole ring resonated as a singlet at δ 5.62 ppm. Seven protons corresponding to sugar moiety resonated between δ 5.90–4.00 ppm. In the ¹³C NMR of 6a, the methylene carbon ($-CH_2-$) was observed at δ 58.60 ppm, while sugar carbons appeared between δ 86.06–61.62 ppm. The HRMS spectrum of 6a exhibited a molecular ion peak at m/z 661.2141 $[M + H]^+$, corresponding to the molecular formula C₃₃H₃₃N₄O₁₁. Further, the structures of compound 6a, 6b, and 6e was confirmed by single-crystal X-ray diffraction (SC-XRD) analyses.

3.2. Anticancer activity

The library of 2-phenylquinoline-triazole-bridged *N*-glycoconjugates 6(a–j) was evaluated for their anticancer potency against MCF-7 cancer cell lines. MTT assay was employed to determine the growth inhibitory effects and reduction in cell viability of MCF-7 cells. Initially, cells were treated with different concentrations of the compounds 6(a–j) (50–200 μ g mL⁻¹) for 48 h, The IC₅₀ value were determined based on the percentage of cell viability, as summarized in (Table 1). Compounds 6c, 6d, 6f, and 6i exhibited weak cytotoxicity, however rest other derivatives were found inactive. The structure activity relationship (SAR) of glycoconjugates 6(a–j) against MCF-7 cells was preliminary analysed with respect to the nature of sugar scaffold and the electronic effect of aryl substituent attached to the quinoline ring. Overall, galactosyl derivatives exhibited enhanced antiproliferative activity corresponding to their glucosyl analogues. Among all the compounds, the compound 6f was the most potent, exhibiting an IC₅₀ value of 108.59 μ M. Notably, the electron donating substituent such as methoxy group provided moderate activity only in glucose derivatives (6c; IC₅₀ = 131.25 μ M) but loses potency in galactose derivatives (6h; IC₅₀ = >200 μ M). In contrast, weak donors like methyl were unfavourable (6e and 6j). Among the electron-withdrawing



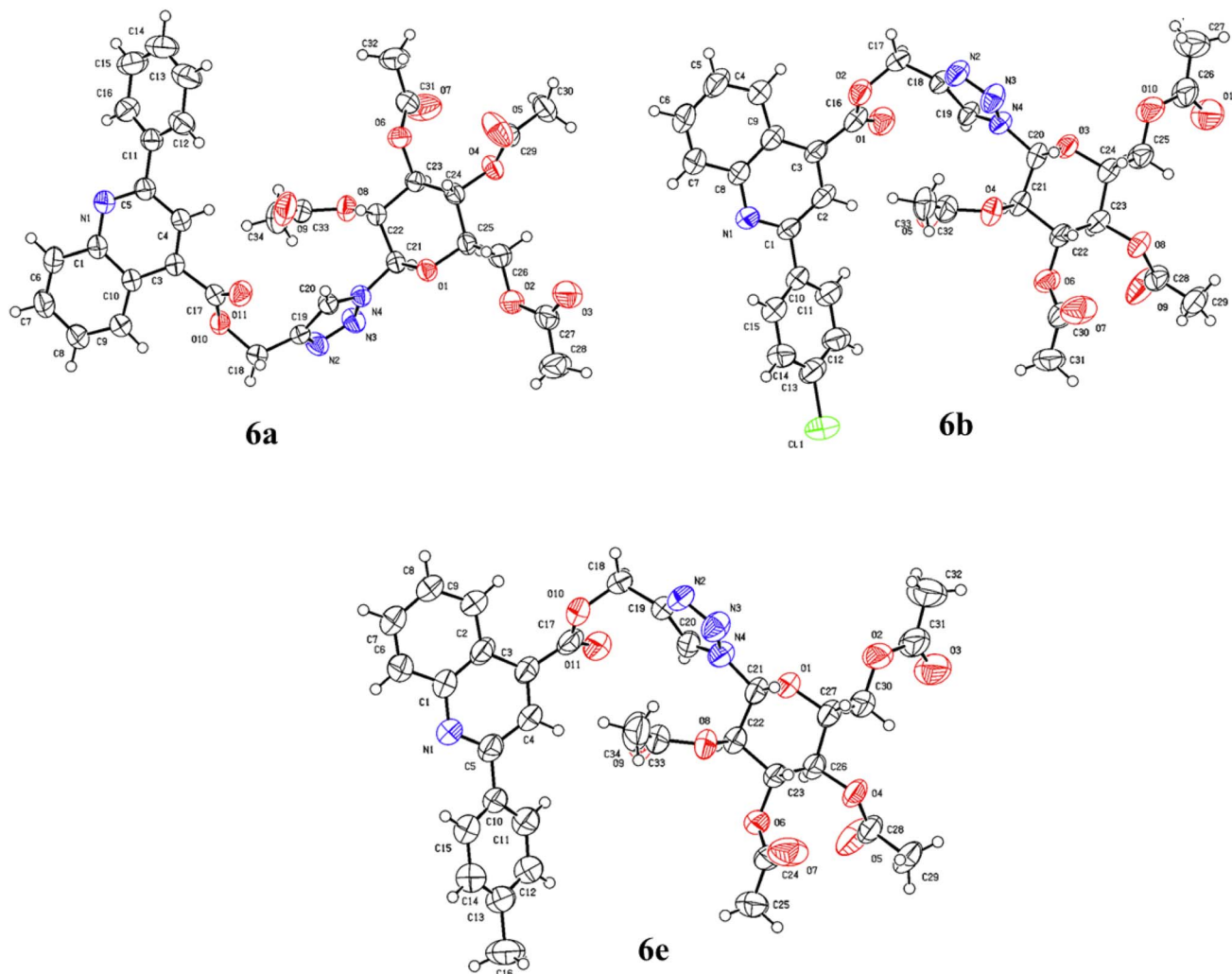


Fig. 2 ORTEP plots showing thermal ellipsoids at 50% probability level.

substituents, fluorine-containing analogues displayed better cytotoxic activity (**6d**; $IC_{50} = 135.95 \mu\text{M}$ and **6i**; $IC_{50} = 151.36 \mu\text{M}$) than their chloro-substituted analogues (**6b** and **6g**). This indicates that substituents exhibiting high electronegativity with minimal steric hindrance are more favourable for activity. The SAR suggests that optimization of the sugar configuration together with electronic effects, steric balance at the 2-aryl quinoline position, is crucial for enhancing anticancer activity.

3.3. Crystal structure description

The compounds **6a**, **6b** and **6e** were crystallized from ethyl acetate and hexane. The diffraction data were obtained to solve their three-dimensional structures. The ortep plot of their thermal probability ellipsoids at 50% probability were given in (Fig. 2). The details of crystal structure solution and refinement are given in (Table 2). In compounds **6a**, **6b** and **6e** the quinoline and triazole ring exhibit a non-coplanar orientation. Additionally, the β -anomeric configuration of the sugar ring was confirmed through analysis of the torsional angles at the anomeric centre.³¹ For the compound **6a**, the torsional angles

$C23-C22-C21-N4$ and $C25-O1-C21-N4$ were found to be -176.7° and 167.1° , respectively. In compound **6b**, the corresponding torsional angles $C22-C21-C20-N4$ and $C24-O3-C20-N4$ were -177.4° and 165.5° , respectively. Similarly, compound **6e** exhibited torsional angles of -177.5° for $C23-C22-C21-N4$ and 167.0° for $C27-O1-C21-N4$. The values of these dihedral angles, being close to 180° , clearly indicate a β -anomeric orientation of the sugar ring in all three compounds **6a**, **6b**, and **6e**. Furthermore, the presence of sp^3/sp^2 C-H \cdots N/O and N-H \cdots N interaction along with hydrogen bonding is illustrated in (Fig. 3–5). The details of other crucial non covalent interaction that contributed significantly to the crystal packing stabilization of the compounds **6a**, **6b**, and **6e** are summarized in the form of a table (ESI, Table S1).

3.4. Molecular docking analysis

Molecular docking analyses were performed for the most potent compounds **6c**, **6d**, and **6f** to explore their binding interactions and potential inhibitory mechanisms against the ER α enzyme (PDB ID: 3ERT). Normally, ER α activity is precisely controlled;



Table 2 Crystal data and structure refinement details

| Compound | 6a | 6b | 6c |
|--|---|--|---|
| Empirical formula | C ₃₃ H ₃₂ N ₄ O ₁₁ | C ₃₃ H ₃₁ ClN ₄ O ₁₁ | C ₃₄ H ₃₄ N ₄ O ₁₁ |
| Formula weight | 660.62 | 695.07 | 674.65 |
| Temperature | 293 K | 293 K | 298 K |
| Crystal system | Triclinic | Triclinic | Triclinic |
| Space group | <i>P</i> 1 | <i>P</i> 1 | <i>P</i> 1 |
| Unit cell dimensions | <i>a</i> = 5.7948 (10) Å <i>b</i> = 11.9278 (2) Å <i>c</i> = 12.1042 (2) Å α = 82.636 (2)° β = 87.276 (10)° γ = 81.538 (2)° | <i>a</i> = 5.8670 (2) <i>b</i> = 12.0574 (4) <i>c</i> = 12.1900 (4) α = 81.389 (3) β = 80.238 (3)° γ = 86.153 (3) | <i>a</i> = 5.8582 (3) <i>b</i> = 12.1432 (5) <i>c</i> = 12.2428 (4) α = 81.207 (3) β = 80.608 (3)° γ = 86.419 (4)° |
| Volume | 818.14 (2) Å ³ | 839.50 (5) Å ³ | 848.93 (6) Å ³ |
| Z | 1 | 1 | 1 |
| Density (calculated) | 1.341 g cm ⁻³ | 1.375 g cm ⁻³ | 1.320 g cm ⁻³ |
| Absorption coefficient | 0.858 mm ⁻¹ | 1.580 mm ⁻¹ | 0.838 mm ⁻¹ |
| <i>F</i> (0 0 0) | 346.0 | 362.0 | 354.0 |
| Theta range for data collection | 7.366°–135.926° | 7.422°–136.502° | 7.372°–144.198° |
| Index ranges | −6 ≤ <i>h</i> ≤ 6 −14 ≤ <i>k</i> ≤ 14 −13 ≤ <i>l</i> ≤ 14 | −7 ≤ <i>h</i> ≤ 7 −11 ≤ <i>k</i> ≤ 14 −14 ≤ <i>l</i> ≤ 14 | −7 ≤ <i>h</i> ≤ 7 −14 ≤ <i>k</i> ≤ 14 −15 ≤ <i>l</i> ≤ 15 |
| Reflections collected | 11 155 | 7523 | 8284 |
| Independent reflections | 4237 [<i>R</i> (int) = 0.0202] | 3851 [<i>R</i> (int) = 0.0758] | 4008 [<i>R</i> (int) = 0.039] |
| Absorption correction | 'Multi-scan' | 'Multi-scan' | 'Multi-scan' |
| Refinement method | Full-matrix least-squares on <i>F</i> ² | Full-matrix least-squares on <i>F</i> ² | Full-matrix least-squares on <i>F</i> ² |
| Data/restraints/parameters | 4237/3/437 | 3851/3/446 | 4008/3/448 |
| Goodness-of-fit on <i>F</i> ² | 1.058 | 1.196 | 1.185 |
| Final <i>R</i> indices | <i>R</i> ₁ = 0.0332, <i>wR</i> ₂ = 0.0823 | <i>R</i> ₁ = 0.0905, <i>wR</i> ₂ = 0.2669 | <i>R</i> ₁ = 0.0908, <i>wR</i> ₂ = 0.2972 |
| <i>R</i> Indices (all data) | <i>R</i> ₁ = 0.0342 <i>wR</i> ₂ = 0.0834 | <i>R</i> ₁ = 0.1060 <i>wR</i> ₂ = 0.2917 | <i>R</i> ₁ = 0.1094 <i>wR</i> ₂ = 0.3171 |
| Largest diff. Peak and hole | 0.12/−0.17 e Å ⁻³ | 0.48/−0.48 e Å ⁻³ | 0.41/−0.36 e Å ⁻³ |
| CCDC number | 2457702 | 2424982 | 2445773 |

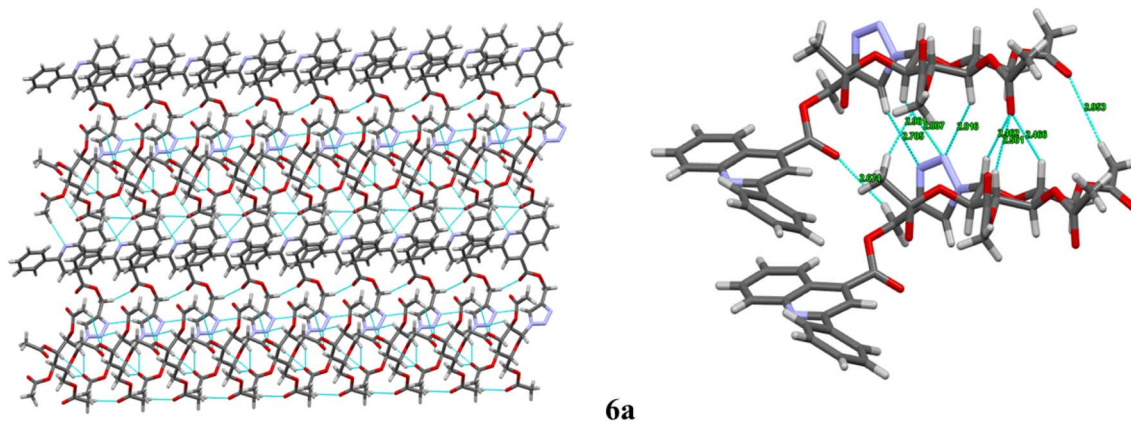


Fig. 3 Intermolecular interaction along with hydrogen bonding between C–H, N–H...N, C–H...N, and C–H...O (sp², sp³) along *b* axis of molecule 6a.

however, its dysregulation in various cancer types contributes to unchecked cellular proliferation, genomic instability, and tumour development. Tamoxifen acts as a selective ER α modulator that binds to the receptor's ligand-binding domain, blocking estrogen-mediated transcriptional activation and thereby suppressing cancer cell growth. Consequently, the crystal structure of the human estrogen receptor alpha (ER α) ligand-binding domain complexed with 4-hydroxytamoxifen

was utilized for the docking studies. The 2-phenylquinoline triazole glycoconjugates **6c**, **6d**, and **6f** displayed strong binding affinity within the ER α active site, with docking energies of −9.1, −9.5 and 8.9 kcal mol⁻¹, respectively (ESI, Table S2). To confirm the reliability of the docking procedure, the native co-crystallized ligand, 4-hydroxytamoxifen, was re-docked into the ER α active site, resulting a docking score of −9.7 kcal mol⁻¹ and an RMSD value of 1.514 Å. The close alignment of the re-



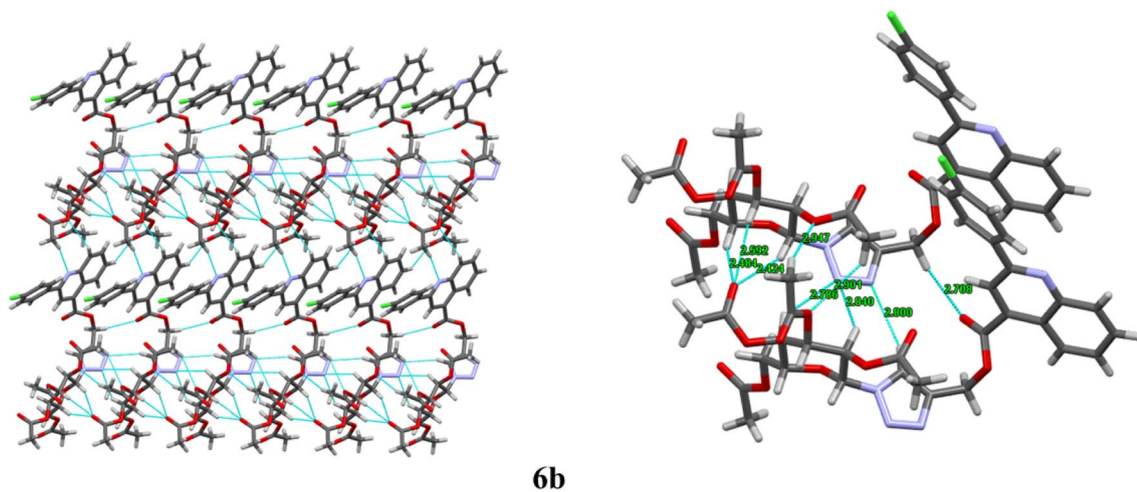


Fig. 4 Intermolecular interaction along with hydrogen bonding between (C–H, N–H...N, C–H...N, and C–H...O)(sp², sp³) along *b* axis of **6b**.

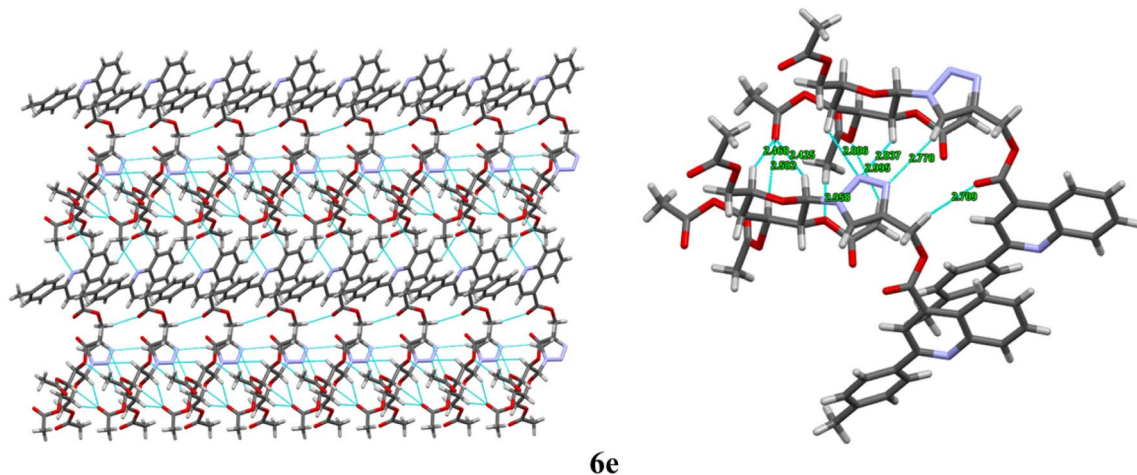


Fig. 5 Intermolecular interaction along with hydrogen bonding between (C–H, N–H...N, C–H...N, and C–H...O) (sp², sp³) along *b* axis of **6e**.

docked conformation with the experimentally determined binding poses further validated the accuracy and robustness of the docking protocol (Fig. S62).

Compound **6c** displayed a strong affinity and was stabilized within the ER α active site by a hydrogen bond between the acetoxy oxygen of the 6-acetyl group on the sugar moiety and Leu536, along with a π -sulfur interaction between the triazole nitrogen and Cys530. Additional stabilization arose from π -alkyl and alkyl interactions involving the methoxyphenyl, quinoline and triazole rings with residues Ala350, Leu525, and Val533, as well as an interaction between the methoxy substituent and Leu346. A π -anion interaction between Asp351 and the quinoline ring as well as multiple van der Waals contacts with surrounding residues collectively contributed to the overall stability of the **6c**-ER α complex (Fig. 6).

The compound **6d** formed stable complex with ER α via a hydrogen bond interaction between the fluorine atom and Arg394, along with a halogen interaction with the Leu387 residue. Quinoline nucleus showed π -alkyl interactions with

Met421 and Met343, whereas the phenyl substituent of quinoline scaffold interacted with Leu391. Moreover, Leu525 formed π -sigma contacts with both the quinoline and triazole cores, and Leu346 involved π -alkyl interactions with the quinoline and fluorophenyl rings. Additionally, van der Waals contacts with neighbouring residues further enhanced the stability of compound **6d** with receptor (Fig. 6).

Similarly, compound **6f** established favourable binding interactions with receptor ER α through two hydrogen bonds between the acetoxy oxygens of the 6-acetyl and 3-acetyl groups on the sugar moiety and the amino acid residues Leu536 and Trp383, respectively. The binding was further stabilized by π -alkyl interactions involving the quinoline and triazole moieties with Ala350, Leu525, and Lys529 residues. Furthermore, a π -anion interaction between Asp351 and the quinoline framework along with several van der Waals interactions contributed a stable **6f**-ER α association (Fig. 6).

Despite the favourable molecular docking scores of compounds **6c**, **6d**, and **6f** against ER α , their *in vitro*



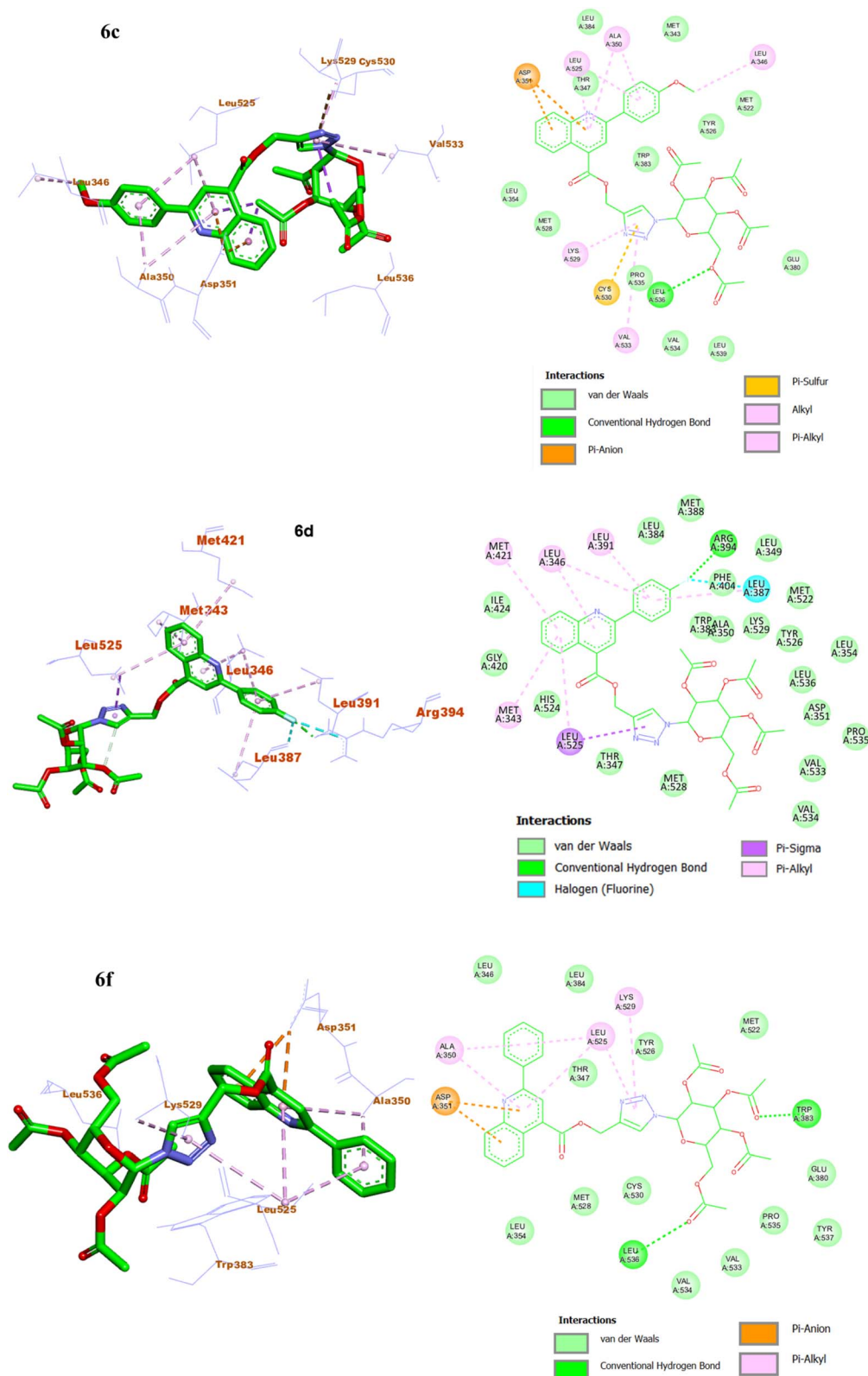


Fig. 6 The 3D and 2D bindings mode of compound 6f, 6c, and 6d within the active site of ER α .

antiproliferative activity against the MCF-7 cell line was poor. This discrepancy may be attributed to inherent limitations of molecular docking, which does not fully account for receptor dynamics, solvation, solubility, cellular uptake, or metabolic

stability, and often shows limited correlation with experimental potency. Accordingly, these compounds may be considered preliminary leads, warranting further structure-guided optimization to improve biological activity.³²



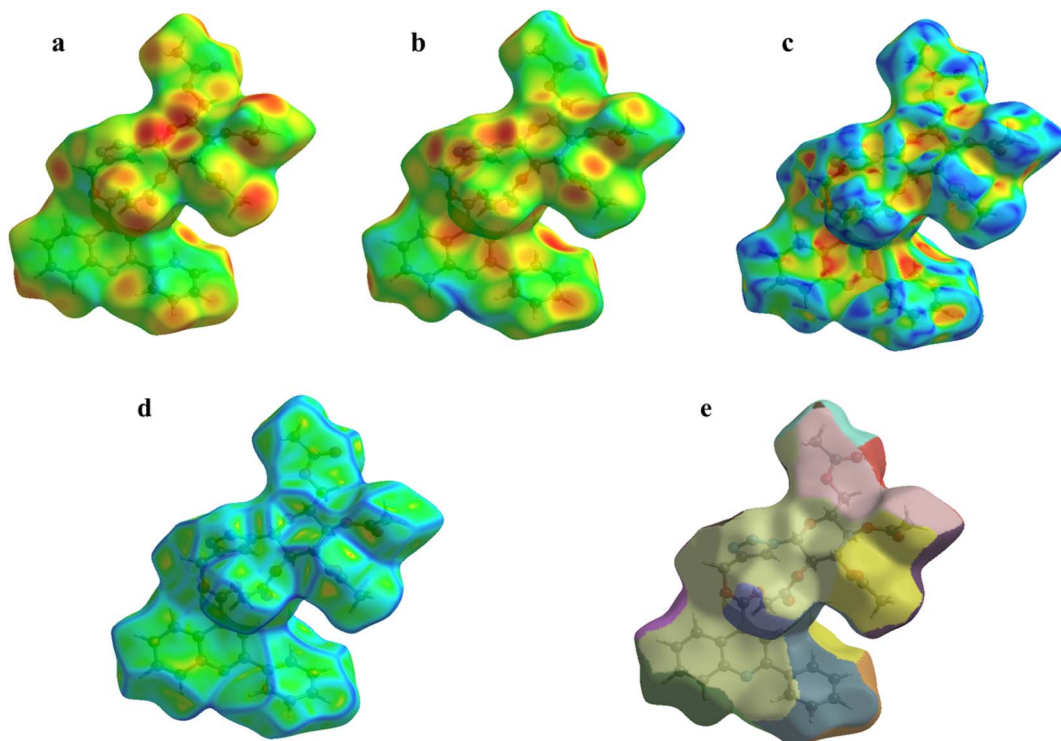


Fig. 7 (a) di (b) de (c) shape index (d) curvedness (e) fragment Patch along the *b*-axis of the compound 6a.

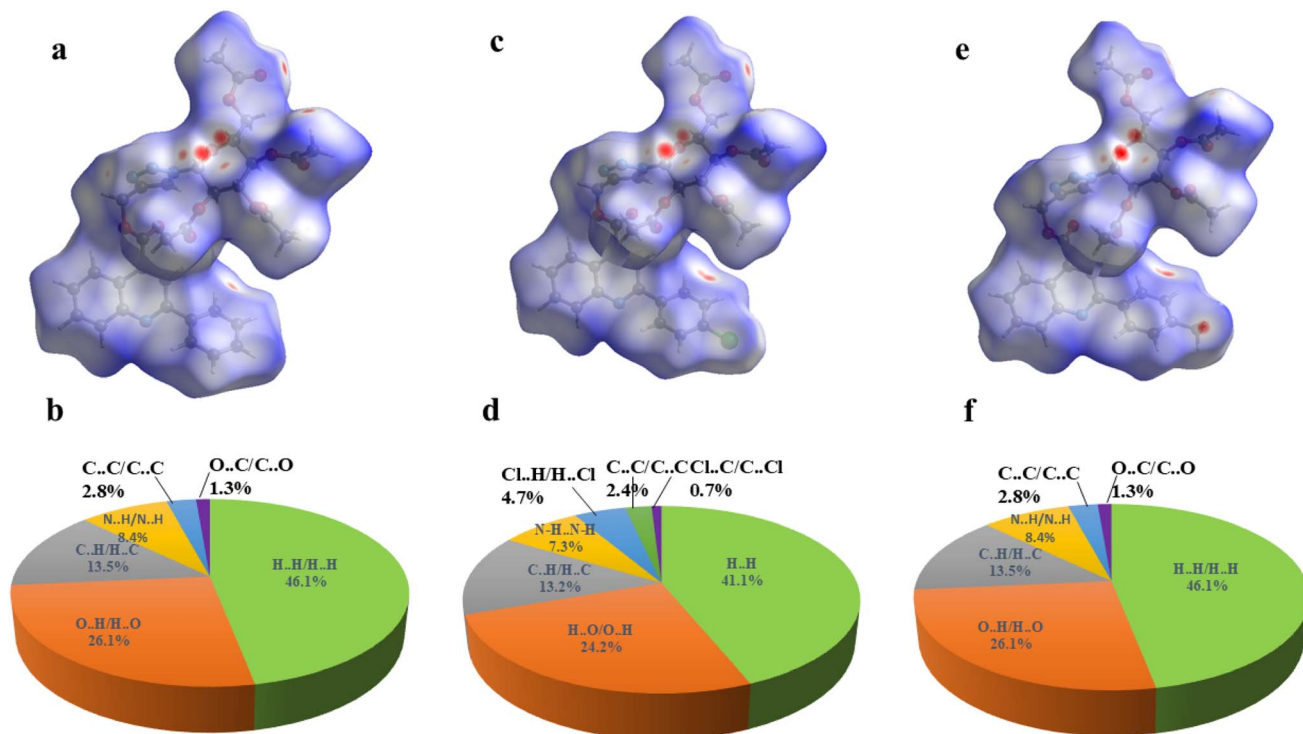


Fig. 8 d_{norm} surfaces and 2D fingerprint plots for 6a (a and b), 6b (c and d), and 6e (e and f). Pie chart representing the percentage contributions of different 2d Finger interactions in the Hirshfeld surface.



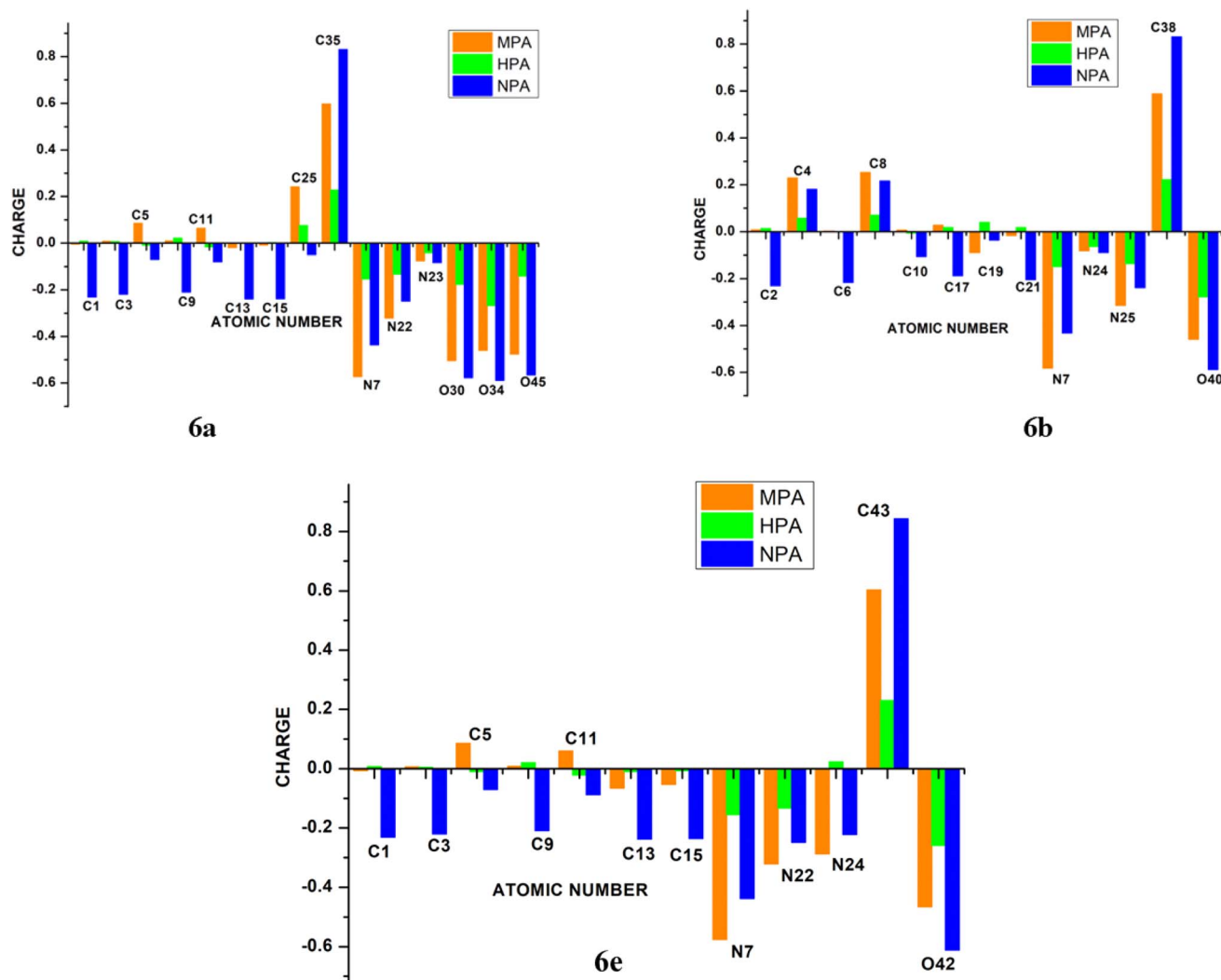


Fig. 10 Atomic charge presentation at the selected atoms in **6a**, **6b**, and **6e** based on MPA, HPA, and NPA charge schemes.

summarized in ESI, Table S3. The computed quantities include zero-point vibrational energy (ZPVE), thermal corrections to energy, enthalpy, and Gibbs free energy, as well as the total electronic energy and the sums of electronic and thermal energies, enthalpies, and free energies. Other relevant thermodynamic parameters, such as total entropy and heat capacity at constant volume, were also determined. The calculated entropy values, which provide insight into molecular flexibility and disorder relevant to binding behaviour, were found to be $275.04 \text{ cal mol}^{-1} \text{ K}^{-1}$ for compound **6a**, $286.332 \text{ cal mol}^{-1} \text{ K}^{-1}$ for **6b**, and $285.82 \text{ cal mol}^{-1} \text{ K}^{-1}$ for **6e**.

3.6.2. Atomic charge analysis. Effective atomic charges for compounds **6a**, **6b**, and **6e** were evaluated using Mulliken (MPA), Hirshfeld (HPA), and Natural Population Analysis (NPA) at the B3LYP/6-31G(d,p) level in the gas phase (Fig. 10). Although atomic charges are not directly observable, they provide valuable insight into molecular polarity, electronic distribution, and reactivity. While MPA is computationally efficient, it is highly basis-set dependent, whereas HPA and NPA yield more consistent charge distributions, with NPA typically

producing larger charge magnitudes. Accordingly, NPA results were primarily considered for discussion.³⁴ According to the NPA results, the C35 atom exhibited the highest positive charge (0.830 a.u.) in compound **6a**, while in compound **6b** the C38 atom showed the maximum positive charge (0.831 a.u.). For compound **6e**, the most positively charged atom was C43, with a value of 0.603 a.u. In all three compounds, the atoms carrying the highest positive charges correspond to the carbonyl carbon atoms of the acetyl sugar moieties. These high positive charges are attributed to the influence of the nearby electronegative oxygen atoms of the acetyl groups, specifically O34 and O33 in **6a**; O40 and O37 in **6b**; and O42 and O41 in **6e**. Several atoms in each compound displayed negative charges. In compound **6a**, the negatively charged atoms included N7, N22, N23, C1, C3, C9, C13, and C15. In compound **6b**, negatively charged atoms were identified as C2, C6, C10, C17, C19, C21, N7, N24, and N25. For compound **6e**, the atoms with negative charges were C1, C3, C9, C13, C15, O42, N7, N22, and N24. Among all atoms, the three oxygen atoms O30, O34, and O45 in compound **6a**, O40 in **6b**, and O42 in **6e** exhibited notably high negative charges in

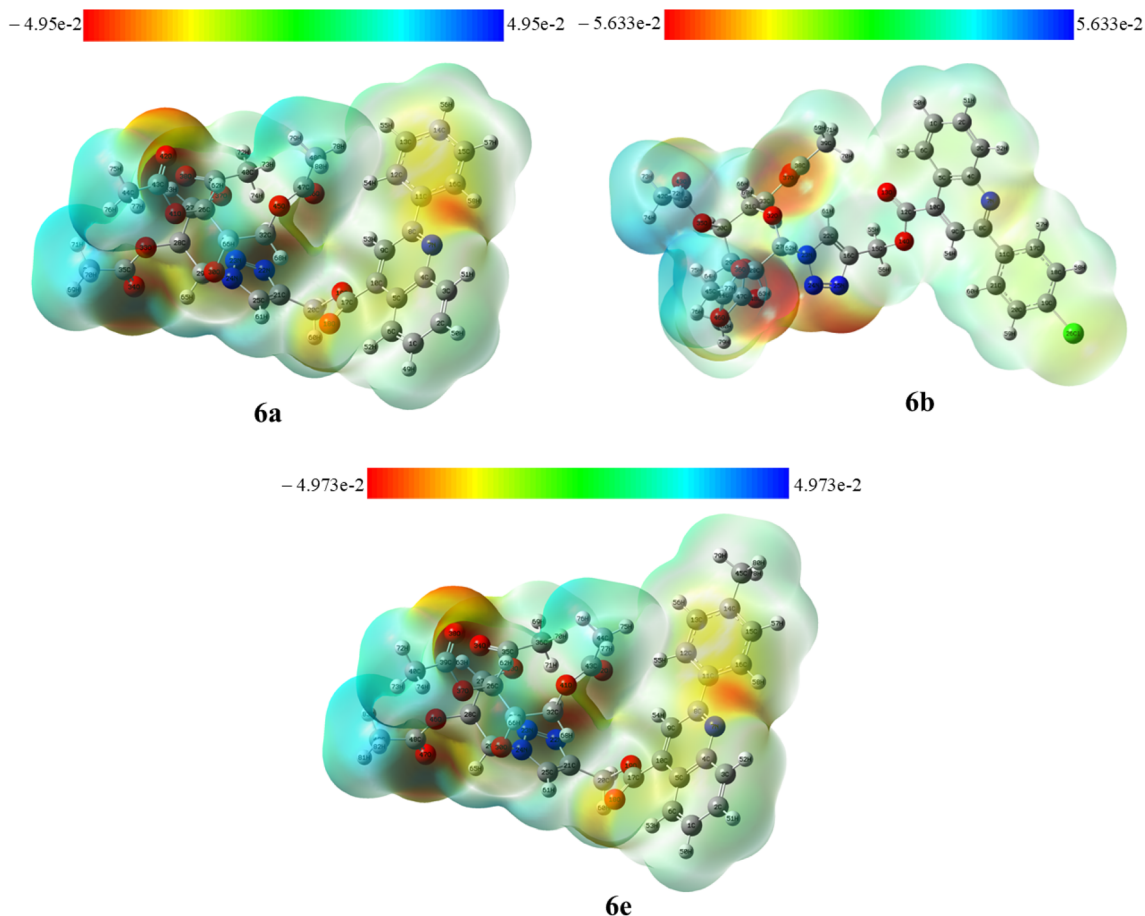


Fig. 11 Molecular electrostatic potential (MEP) of the 1,2,3-triazole linked quinoline glycoconjugates **6a**, **6b** and **6e** in the gas phase.

their neutral states. These oxygen atoms were identified as the most basic sites in their respective molecules.

3.6.3. Molecular electrostatic potential. The Molecular Electrostatic Potential (MEP) represents the spatial distribution of electrostatic potential produced by the combined influence of the atomic nuclei and the surrounding electron cloud. It helps visualize how charge is arranged across a molecule and identifies electron-rich (negative, red), electron-poor (positive, blue), and neutral (green) regions. In the colour mapping sequence red \rightarrow orange \rightarrow yellow \rightarrow green \rightarrow blue, the potential increases correspondingly. MEP mapping serves as an essential computational approach for assessing reactivity trends, molecular recognition patterns, and drug–target interactions.³⁵ The MEP surfaces of compounds **6a**, **6b**, and **6e** were generated in the gas phase using B3LYP/6-31G(d,p) optimized geometries (Fig. 11). The potential ranges were -4.95×10^{-2} to 4.95×10^{-2} a.u. for **6a**, -5.633×10^{-2} to 5.633×10^{-2} a.u. for **6b**, and -4.973×10^{-2} to 4.973×10^{-2} a.u. for **6e**. In compounds **6a** and **6e**, the carbonyl oxygen of the acetylated sugar, oxygens (O18 and O19) near the coumarin ring, and nitrogens of the triazole and quinoline rings showed high electron density areas favourable for electrophilic attack. In **6b**, similar red regions were observed near the acetyl carbonyl oxygen and the triazole-quinoline nitrogen's, reflecting comparable charge localization.

Conversely, the methyl groups attached to the acetylated sugar in all three molecules were visualized in blue, denoting electron-deficient centers susceptible to nucleophilic attack.

3.6.4. Global reactivity descriptors. Global reactivity parameters derived from conceptual Density Functional Theory (DFT) were evaluated for the ground-state optimized geometries of compounds **6a**, **6b**, and **6e** in the gas phase, and the corresponding results are summarized in Fig. 12, Table 3. In molecular orbital theory, the Highest Occupied Molecular Orbital (HOMO) represents the electron-donating ability of a molecule and is linked to the ionization potential, whereas the Lowest Unoccupied Molecular Orbital (LUMO) acts its electron-accepting capacity and correlates with the electron affinity.³⁶ The HOMO–LUMO energy difference (ΔE) serves as an indicator of electronic stability and reactivity; a larger gap denotes greater molecular stability and lower reactivity, while a smaller gap suggests enhanced chemical responsiveness.³⁷ These electronic indices are widely employed to describe drug–receptor interaction sites and binding behaviour. According to frontier molecular orbital (FMO) theory, the biological response of a compound is significantly influenced by its HOMO–LUMO energy gap. In the present study, compounds **6a**, **6b**, and **6e** displayed nearly identical and relatively large HOMO–LUMO energy gaps (~ 7 eV), indicating low molecular reactivity.



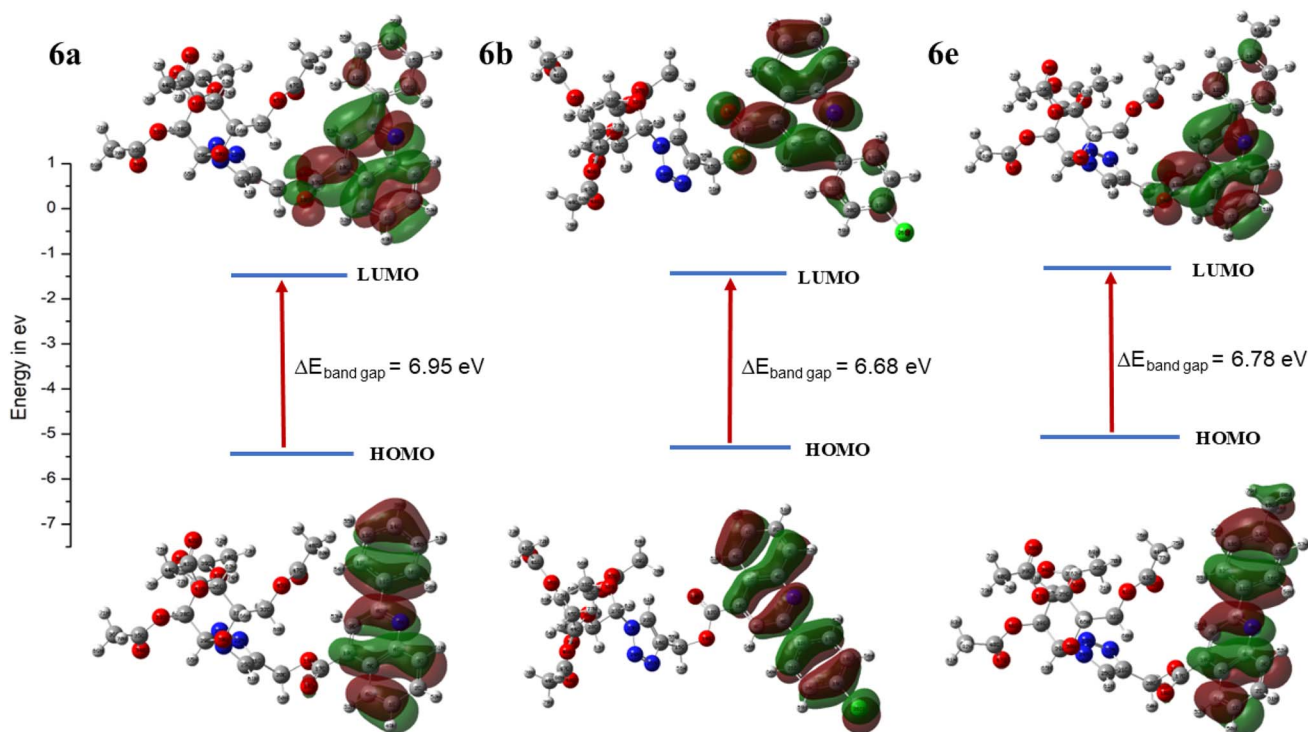


Fig. 12 Frontier molecular orbitals contributing in electronic absorption along with band gap (ΔE) of compounds **6a**, **6b** and **6e** calculated at B3LYP/6-31G (d,p) level of theory.

Table 3 Global reactivity descriptors for compound **6a**, **6b** and **6e**

| Compounds | Dipole moment (debye) ^a | I.P. (eV) ^b | E.A. (eV) ^c | HOMO (eV) | LUMO (eV) | ΔE (eV) | μ (eV) ^d | χ (eV) ^e | η (eV) ^f | S (1/eV) ^g | ω (eV) ^h |
|-----------|------------------------------------|------------------------|------------------------|-----------|-----------|-----------------|-------------------------|--------------------------|--------------------------|-------------------------|----------------------------|
| 6a | 5.10 | 7.51 | 0.57 | -7.51 | -0.57 | 6.95 | -4.04 | 4.05 | 3.47 | 0.28 | 2.36 |
| 6b | 8.49 | 7.60 | 0.91 | -7.60 | -0.91 | 6.68 | -4.25 | 4.25 | 3.34 | 0.29 | 2.71 |
| 6e | 4.71 | 7.34 | 0.56 | -7.34 | -0.56 | 6.78 | -3.95 | 3.95 | 3.40 | 0.30 | 2.30 |

^a Dipole moment for the system containing N number of electrons. ^b Ionization potential (I.P.) = $E_{N-1} - E_N$. ^c Electron affinity (E.A.) = $E_N - E_{N+1}$.

^d Electronic chemical potential (μ) = $\frac{E_{\text{HOMO}} + E_{\text{LUMO}}}{2}$ [$-E_{\text{HOMO}}$ = I.P. and $-E_{\text{HOMO}} - E.A.$]. ^e Electronegativity (χ) = $\frac{\text{I.P.} + \text{E.A.}}{2}$. ^f Global hardness

(η) = $\frac{\text{I.P.} - \text{E.A.}}{2}$. ^g Global softness (S) = $1/(2\eta)$. ^h Electrophilicity index (ω) = $\mu^2/(2\eta)$.

Notably, all three compounds exhibited poor cytotoxic activity, with IC_{50} values greater than 200 μM . This reduced biological performance can be attributed to the large energy gap, which likely limits efficient electronic interactions with biological targets.³⁸

Conversely, a molecule with higher global hardness exhibits a greater resistance to changes in its electronic distribution during chemical reactions.³⁶ The calculated global hardness (η) values for compounds **6a**, **6b**, and **6e**, ranging from 3.3 to 3.5 eV, indicate that these molecules possess a significant resistance to charge transfer processes. The electronegativity (χ) of a molecule reflects its tendency to attract electrons, while a more negative chemical potential (μ) generally corresponds to enhanced stability in receptor binding.³⁹ The studied compounds exhibit notably negative chemical potentials (-3.95 to -4.25 eV), suggesting higher sensitivity to variations in electron number and a stronger propensity to form stable

interactions with biological targets. Furthermore, the electrophilicity index (ω) values for compounds **6a**, **6b**, and **6e**, ranging from 2.30–2.71 eV, indicate a strong tendency to accept electrons from biomolecular receptors, thereby enhancing potential receptor interactions. The calculated dipole moments further support these findings, with compound **6b** displaying the highest value (8.49 D) compared to **6a** (5.10 D) and **6e** (4.71 D), implying a greater degree of charge separation within its molecular framework and, consequently, stronger polar interactions with receptor sites.

3.6.5. Local reactivity descriptor. The NPA charge distribution was employed to evaluate the Fukui functions, which serve as local reactivity indicators, for specific atoms in compounds **6a**, **6b**, and **6e** that participate in binding interactions with the ER α receptor during docking studies. The Fukui function $f^-(k)$ represents an atom's ability to accept electrons, signifying its potential involvement with nucleophilic (electron-



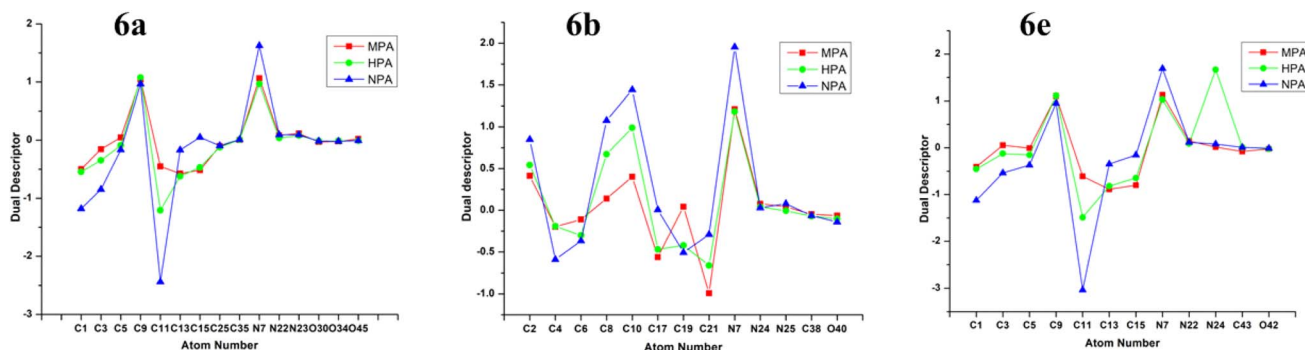


Fig. 13 Variation of dual descriptor, at the selected atoms of compounds **6a**, **6b** and **6e** based on MPA, HPA, and NPA charges based, calculated at B3LYP/6-31G (d,p) level of theory (eV).

rich) residues, whereas $f^-(k)$ characterizes the electron-donating ability of an atom, indicating its possible interaction with electrophilic (electron-deficient) residues.³⁶ The dual descriptor was determined using the expression $f^2(k) = [f^+(k) - f^-(k)]$, which provides an integrated perspective on whether an atom preferentially donates or accepts electrons.⁴⁰ A positive $f^2(k)$ value designates an atom as an electron acceptor (electrophilic site), while a negative value indicates an electron donor (nucleophilic site). This analysis aids in pinpointing the reactive centers within each molecule that are likely to engage in electronic interactions with the receptor residues. The computed results revealed that, in both **6a** and **6e**, atoms such as C9 and N7 exhibited positive $f^2(k)$ values, identifying them as electrophilic centers, while C1, C3, and C11 displayed negative $f^2(k)$ values, suggesting their nucleophilic character. Additionally, atoms O30, O34, and O45 in **6a**, O40 in **6b**, and O42 in **6e** were recognized as moderately reactive sites, likely contributing to complex stabilization through hydrogen bonding interactions. In compound **6b**, the atoms C8, C10, and N7 were identified as preferred nucleophilic centers, whereas C4, C6, and C21 were characterized as electrophilic sites (Fig. 13).

3.6.6. Natural bond orbital analysis (NBO). The NBO study for compounds **6a**, **6b**, and **6e** was carried out at the B3LYP/6-31G(d,p) level of theory in the gas phase to investigate the intramolecular charge transfer (ICT) phenomena (ESI, Tables S4–S6). The analysis was based on the second-order perturbation theory of the Fock matrix, which quantifies the donor-acceptor interactions in terms of the associated stabilization energy $E^{(2)}$. Higher $E^{(2)}$ values signify more efficient electron delocalization between bonding and antibonding orbitals, indicating strong hyperconjugative effects and enhanced electronic communication within the molecular system.⁴¹ The results of NBO analysis showing a significant hyperconjugative interactions: LP(2)O19 \rightarrow $\pi^*(C17-O18)$, LP(2)O41 \rightarrow $\pi^*(O42-C43)$, LP(2)O33 \rightarrow $\pi^*(O34-C35)$, LP(1)N24 \rightarrow $\pi^*(N22-N23)$, LP(2)O37 \rightarrow $\pi^*(O38-C39)$, LP(2)O34 \rightarrow $\sigma^*(O33-C35)$, LP(2)O38- $\sigma^*(O37-C39)$, LP(2)O42 \rightarrow $\sigma^*(O41-C43)$, in both **6a** and **6e**. Some more high energy hyperconjugative interactions were LP(2)O45 \rightarrow $\pi^*(O46-C47)$, LP(2)O46 \rightarrow $\sigma^*(O45-C47)$ in **6a** and LP(2)O46 \rightarrow $\pi^*(O47-C48)$, LP(2)O47 \rightarrow $\sigma^*(O46-C48)$ in **6e**. The most prominent interactions in compound **6b** were LP(2)O14

\rightarrow $\pi^*(C12-O13)$, LP(2)O36 \rightarrow $\pi^*(C44-O46)$, LP(2)O35 \rightarrow $\pi^*(C41-O43)$, LP(2)O37 \rightarrow $\pi^*(C38-O40)$, LP(1)N23 \rightarrow $\pi^*(N24-N25)$, LP(2)O13 \rightarrow $\sigma^*(C12-O14)$, LP(2)O40 \rightarrow $\sigma^*(O37-C38)$, LP(2)O43 \rightarrow $\sigma^*(O35-C41)$, LP(2)O46 \rightarrow $\sigma^*(O36-C44)$, LP(2)O48 \rightarrow $\sigma^*(O34-C47)$. Other high energy stabilization interactions are $\pi^*(N7-C8) \rightarrow \pi^*(C9-C10)$, $\pi(C21-C25) \rightarrow \pi^*(N22-N23)$, $\pi(C9-C10) \rightarrow \pi^*(N7-C8)$, $\pi(C15-C16) \rightarrow \pi^*(C13-C14)$, in both **6a** and **6e**, and $\pi^*(N7-C8) \rightarrow \pi^*(C9-C10)$, $\pi(C16-C22) \rightarrow \pi^*(N24-N25)$, and $\pi(C9-C10) \rightarrow \pi^*(C12-O13)$, $\pi(C11-C21) \rightarrow \pi^*(C19-C20)$, $\pi(N7-C8) \rightarrow \pi^*(C4-C5)$, in **6b**.

4. Conclusion

A novel series of phenyl-substituted quinoline-1,2,3-triazole glycoconjugates (**6a–6k**) was efficiently synthesized using a Cu(I)-catalyzed azide-alkyne cycloaddition (CuAAC) strategy, demonstrating the versatility of this approach for incorporating diverse sugar azides to phenyl-substituted quinoline precursors. The synthesized glycoconjugates were fully characterized by spectroscopic techniques, and the structures of selected derivatives (**6a**, **6b**, and **6e**) were unequivocally confirmed through single-crystal X-ray diffraction. Crystallographic analysis revealed that intermolecular hydrogen-bonding interactions play a significant role in stabilizing the crystal packing. *In vitro* evaluation against the MCF-7 breast cancer cell line revealed that, while most compounds were inactive, a few derivatives (**6f**, **6c**, and **6d**) exhibited weak cytotoxicity, indicating the need for further structural optimization to enhance biological activity. Molecular docking studies showed favourable binding interactions with estrogen receptor alpha (ER α), supporting their potential as ER α -interacting scaffolds. Complementary DFT analyses provided detailed insights into the electronic structure, stability, reactivity, and charge distribution of the compounds, contributing to a deeper understanding of their chemical behaviour.

Conflicts of interest

The authors declare that the research was conducted in the absence of any commercial or financial relationships that could be construed as a potential conflict of interest.



Data availability

CCDC 2457702, 2424982 and 2445773 contain the supplementary crystallographic data for this paper.^{42a-c}

All data supporting the findings of this study are provided in the supporting information (SI). Supplementary information: including detailed experimental procedures, complete characterization data, NMR and HRMS spectra, X-ray crystallographic analyses, and DFT computational results. See DOI: <https://doi.org/10.1039/d5ra09700b>.

Acknowledgements

D. K. gratefully acknowledges the University Grants Commission (UGC), New Delhi, for the Start-Up Research Grant (M-14-57; Letter No. F.30-431/2018), and the Institute of Eminence (IoE) Seed Grant, Banaras Hindu University (Development Scheme No. 6031), for financial support. R. K. acknowledges UGC for the award of a Senior Research Fellowship. The authors are thankful to Prof. Sandeep Pokharia for his valuable assistance with the DFT studies.

References

- 1 B. S. Matada, R. Pattanashettar and N. G. Yernale, *Bioorg. Med. Chem.*, 2021, **32**, 115973.
- 2 V. Pradhan, R. Kumar, A. Mazumder, M. M. Abdullah, M. Shahar Yar, M. J. Ahsan and Z. Ullah, *Chem. Biol. Drug Des.*, 2023, **101**, 977–997.
- 3 M. F. A. Mohamed and G. E.-D. A. Abu-Rahma, *RSC Adv.*, 2020, **10**, 31139.
- 4 H. C. Kolb, M. G. Finn and K. B. Sharpless, *Angew. Chem., Int. Ed.*, 2001, **40**, 2004–2021.
- 5 C. W. Tornøe, C. Christensen and M. Meldal, *J. Org. Chem.*, 2002, **67**(9), 3057–3064.
- 6 D. Kushwaha and V. K. Tiwari, *J. Heterocycl. Chem.*, 2017, **54**, 2454–2462.
- 7 D. Kushwaha, P. Dwivedi, S. K. Kuanar and V. K. Tiwari, *Curr. Org. Synth.*, 2013, **10**, 90–135.
- 8 D. Kushwaha, S. K. Singh and V. K. Tiwari, *Carbohydr. Drug Discov. Dev.*, 2020, 403–450.
- 9 D. Kushwaha, A. K. Kushwaha, R. Kumar and D. Chauhan, *Bioorg. Chem.*, 2025, **162**, 108559.
- 10 D. Kushwaha, P. Xu and P. Kováč, *RSC Adv.*, 2017, **7**, 7591.
- 11 Y. Zhang, Y. Ji, S. Liu, J. Li, J. Wu, Q. Jin, X. Liu, J. Natl, *et al.*, *Cancer Cent.*, 2025, **5**, 287.
- 12 X. Dai, H. Cheng, Z. Bai and J. Li, *J. Cancer*, 2017, **8**, 3131.
- 13 E. E. Sweeney, R. E. McDaniel, P. Y. Maximov, P. Fan and V. C. Jordan, *Horm. Mol. Biol. Clin. Investig.*, 2012, **9**, 143.
- 14 K. S. S. Praveena, E. V. V. S. Ramarao, N. Y. S. Murthy, S. Akkenapally, C. G. Kumar, R. Kapavarapu and S. Pal, *Bioorg. Med. Chem. Lett.*, 2015, **25**, 1057–1063.
- 15 A. Vultur, J. R. Buettner, J. Kowolik, D. M. Smith, M. B. Bivona, A. A. Kandel, S. Jove and R. Jove, *Mol. Cancer Ther.*, 2008, **7**, 1185–1194.
- 16 M. Krawczyk, A. Kaczmarek, M. Wojciechowski, M. Bednarski, A. Okruszek and A. Cholewiński, *Bioorg. Chem.*, 2019, **84**, 326–338.
- 17 S. Zhou, H. Liao, M. Liu, G. Feng, B. Fu, R. Li, M. Cheng, Y. Zhao and P. Gong, *Bioorg. Med. Chem.*, 2014, **22**, 6438–6452.
- 18 S. Li, Y. Zhao, X. Chen, L. Wang, H. Zhang, J. Liu and Y. Liu, *Eur. J. Med. Chem.*, 2019, **162**, 666–678.
- 19 B. R. Kusuma, A. Khandelwal, W. Gu, D. Brown, W. Liu, G. Vielhauer, J. Holzbeierlein and B. S. Blagg, *Bioorg. Med. Chem.*, 2014, **22**, 1441–1449.
- 20 A. M. Mohassab, A. H. Abdelazeem, H. A. El-Morsy, M. F. Ismail and A. M. Abouzid, *Bioorg. Chem.*, 2021, **106**, 104510.
- 21 D. Verbanac, R. Malik, M. Chand, K. Kushwaha, M. Vashist, M. Matijašić, V. Stepanić, M. Perić, H. Č. Paljetak, L. Saso and S. C. Jain, *J. Enzyme Inhib. Med. Chem.*, 2016, **31**, 104–110.
- 22 W. A. Szarek and J. K. N. Jones, *Can. J. Chem.*, 1965, **43**, 2345–2356.
- 23 J. Eberhardt, D. Santos-Martins, A. F. Tillack and S. Forli, *J. Chem. Inf. Model.*, 2021, **61**, 3891–3898.
- 24 O. Trott and A. O. A. Vina, *J. Comput. Chem.*, 2010, **31**, 455–461.
- 25 D. Kratzert, J. J. Holstein and I. Krossing, *J. Appl. Cryst.*, 2015, **48**, 933–938.
- 26 O. V. Dolomanov, L. J. Bourhis, R. J. Gildea, J. A. Howard and H. Puschmann, *J. Appl. Cryst.*, 2009, **42**, 339–341.
- 27 G. M. Sheldrick, *Acta Crystallogr., Sect. C: Struct. Chem.*, 2015, **71**, 3–8.
- 28 M. J. Frisch *et al.*, *Gaussian 09, Revision D.01*, Gaussian, Inc., Wallingford CT, 2009.
- 29 E. Frisch, J. Millam, B. Nielsen, A. J. Holder, J. Hiscocks and M. J. Frisch, *GaussView, Version 5.8*, Gaussian, Inc., Wallingford CT, 2009.
- 30 A. D. Becke, *J. Chem. Phys.*, 1993, **98**, 5648–5652.
- 31 D. Chauhan, R. Kumar, R. K. Gupta, R. Pratap, P. K. Dubey and D. Kushwaha, *J. Mol. Struct.*, 2025, **1351**, 144243.
- 32 Y. Li, J. Yi, H. Li, K. Li, F. Kang, Y. Deng, C. Wu, X. Fu, D. Jiang and D. Cao, *Chem. Sci.*, 2025, **16**, 17374–17390.
- 33 M. J. Turner, J. J. McKinnon, S. K. Wolff, D. J. Grimwood, P. R. Spackman, D. Jayatilaka and M. A. Spackman, *CrystalExplorer 17.5*, University of Western Australia, Perth, 2022.
- 34 F. Martin and H. Zipse, *J. Comput. Chem.*, 2005, **26**, 97–105.
- 35 P. Politzer, P. R. Laurence and K. Jayasuriya, *Environ. Health Perspect.*, 1985, **61**, 191–202.
- 36 P. Geerlings, F. De Proft and W. Langenaeker, *Theor. Chem. Acc.*, 2020, **139**, 36.
- 37 W. Kohn, A. D. Becke and R. G. Parr, *J. Phys. Chem.*, 1996, **100**, 12974–12980.
- 38 M. Karelson, V. S. Lobanov and A. R. Katritzky, *Chem. Rev.*, 1996, **96**, 1027–1044.
- 39 R. G. Pearson, *Proc. Natl. Acad. Sci. U.S.A.*, 1986, **83**, 8440–8441.
- 40 C. Morell, A. Grand and A. Toro-Labbé, *J. Phys. Chem. A*, 2005, **109**, 205–212.



- 41 A. E. Reed, L. A. Curtiss and F. Weinhold, *Chem. Rev.*, 1988, **88**, 899–926.
- 42 (a) CCDC 2457702: Experimental Crystal Structure Determination, 2026, DOI: [10.5517/ccdc.csd.cc2nhfqj](https://doi.org/10.5517/ccdc.csd.cc2nhfqj); (b)

- CCDC 2424982: Experimental Crystal Structure Determination, 2026, DOI: [10.5517/ccdc.csd.cc2mdd7p](https://doi.org/10.5517/ccdc.csd.cc2mdd7p); (c) CCDC 2445773: Experimental Crystal Structure Determination, 2026, DOI: [10.5517/ccdc.csd.cc2n30xq](https://doi.org/10.5517/ccdc.csd.cc2n30xq).

